

Article

## Evaluation of Two Cloud Parameterizations and Their Possible Adaptation to Arctic Climate Conditions

Daniel Klaus \*, Wolfgang Dorn, Klaus Dethloff, Annette Rinke and Moritz Mielke

Alfred Wegener Institute for Polar and Marine Research, Research Department Potsdam, Telegrafenberg A43, Potsdam D-14473, Germany; E-Mails: wolfgang.dorn@awi.de (W.D.); klaus.dethloff@awi.de (K.D.); annette.rinke@awi.de (A.R.); moritz.mielke@awi.de (M.M.)

\* Author to whom correspondence should be addressed; E-Mail: daniel.klaus@awi.de; Tel.: +49-331-288-2202; Fax: +49-331-288-2178.

Received: 31 May 2012; in revised form: 29 June 2012 / Accepted: 24 July 2012 /

Published: 17 August 2012

---

**Abstract:** Based on the atmospheric regional climate model HIRHAM5, the single-column model version HIRHAM5-SCM was developed and applied to investigate the performance of a relative humidity based (RH-Scheme) and a prognostic statistical cloud scheme (PS-Scheme) in the central Arctic. The surface pressure as well as dynamical tendencies of temperature, specific humidity, and horizontal wind were prescribed from the ERA-Interim data set to enable the simulation of a realistic annual cycle. Both modeled temperature and relative humidity profiles were validated against radio soundings carried out on the 35th North Pole drifting station (NP-35). Simulated total cloud cover was evaluated with NP-35 and satellite-based ISCCP-D2 and MODIS observations. The more sophisticated PS-Scheme was found to perform more realistically and matched the observations better. Nevertheless, the model systematically overestimated the monthly averaged total cloud cover. Sensitivity studies were conducted to assess the effect of modified “tuning” parameters on cloud-related model variables. Two tunable parameters of the PS-Scheme and six tuning parameters contained in the cloud microphysics were analyzed. Lower values of the PS-Scheme adjustment parameter  $\tilde{q}_0$ , which defines the shape of the symmetric beta distribution (acting as probability density function), as well as higher values of the cloud water threshold  $CW_{\min}$  or autoconversion rate  $\gamma_1$  are able to reduce the overestimation of Arctic clouds. Furthermore, a lower cloud ice threshold  $\gamma_{\text{thr}}$ , which controls the Bergeron–Findeisen process, improves model cloudiness and the ratio of liquid to solid water content.

**Keywords:** cloud parameterization; single-column climate model; model evaluation; sensitivity study

---

## 1. Introduction

Clouds play a central role in the Arctic climate system. On the one hand, they reflect solar radiation cooling the Earth's surface (cloud albedo effect), on the other hand, they absorb and (re-)emit terrestrial radiation warming the Earth's surface (cloud greenhouse effect). Following Schneider [1], cloud radiative forcing  $CRF = F_{all} - F_{clr}$  is defined as difference between the net radiative fluxes under all-sky ( $F_{all}$ ) and clear-sky ( $F_{clr}$ ) conditions.  $F_{all}$  is the sum of the net longwave (LW) and shortwave (SW) radiative fluxes, while  $F_{clr}$  denotes those fluxes in a cloud-free but otherwise identical atmosphere.

While SW CRF depends on cloud transmittance, surface albedo, and the solar zenith angle, LW CRF is a function of cloud temperature, height, and emissivity as well as the background moisture (e.g., [2,3]). Furthermore, CRF varies depending on cloud phase, aerosol loading and whether convective or stratiform clouds are treated [4–6]. The radiative effects of clouds and their impact on climate have been addressed in many observational and/or modeling studies. Although Ramanathan *et al.* [7] and Schneider [1] have shown that clouds have a net cooling effect on the global climate, the studies of Walsh and Chapman [8] and Intrieri *et al.* [9] have identified the net warming effect of clouds on the Arctic surface, except for a short period during summer when the cloud albedo effect outweighs the greenhouse effect.

Due to low surface temperatures, especially during polar night when there is no solar insolation, and advection of warmer air, ground-based or elevated temperature inversions occur frequently in the Arctic boundary layer (ABL) as demonstrated by Kahl *et al.* [10] and Zhang *et al.* [11]. Low Arctic temperatures are accompanied by comparably low absolute humidities. Apart from the presence of sufficient water vapor, airborne aerosol particles are prerequisites for cloud formation at normal supersaturations, acting either as cloud condensation nuclei or ice nuclei. Although Arctic air masses are normally cold, comparably dry and unpolluted [12], high-latitudes are mainly characterized by the occurrence of so-called boundary layer clouds (BLCs, [13–15]). These BLCs show large seasonal and interannual variability, which is reversely related to Arctic sea-ice variability [16,17].

A major problem in climate modeling is the subgrid-scale treatment of cloud processes, requiring sophisticated parameterizations that ideally include the whole complexity of cloud microphysics like water phase changes and precipitation processes. One of the most relevant obstacles is the sparse availability of cloud observations, especially in the inner Arctic (e.g., [18]), impeding the formulation of sufficient cloud parameterizations and validation of model results. The deficient representation of model cloudiness [19–22] plays a relevant role in why the net CRF, or more specifically the cloud-radiation feedback [3,23,24], is not definitely understood to date. Solomon *et al.* [25] have concluded that cloud feedbacks represent the largest source of uncertainty in climate sensitivity estimates. A particular shortcoming in modeling the Arctic climate is the limited representation of prevailing mixed-phase BLCs (e.g., [26–28]). Climate models have also difficulties in accurately modeling the vertical structure

of Arctic clouds associated with the presence of multiple cloud layers, a strong temperature inversion accompanied by rapid moisture decrease above cloud top, and vertical fluxes within the cloud that are decoupled from the surface fluxes [26,29]. All that complicates the determination of surface radiation fluxes, which are very sensitive to the modeled cloud microphysical characteristics. An intercomparison of Arctic regional climate models (RCMs) has confirmed the large uncertainty in simulated cloud cover [30].

However, various Arctic-specific studies (e. g., [31,32]) have identified sources of error, e. g., that layered cloud formation requires a higher-order ABL parameterization. The cloud droplet radius has been found to impact surface LW CRF significantly by changing the emissivity of Arctic clouds [33,34], where the liquid component of mixed-phase clouds dominates radiative properties in general. For the liquid phase Morrison *et al.* [35] have found in part reasonable agreement between modeled and observed microphysical properties of Arctic mixed-phase clouds, while the ice microphysical properties have been identified as significantly biased. Morrison and Pinto [27] have demonstrated that only two-moment bulk microphysical schemes enable the adequate simulation of ice nucleation and snow formation. On the one hand, Morrison *et al.* [36] have shown that these more sophisticated schemes can better reproduce the observed ratio of liquid and solid water in Arctic clouds; on the other hand, these schemes contain plenty of “tuning” parameters derived from lower-latitude measurements which might be inapplicable to Arctic climate conditions.

Convective and stratiform clouds differ considerably in their formation, characteristics (e. g., vertical wind speed, lifetime, horizontal/vertical extent), and generation of precipitation, arguing for individual parameterizations in climate models. Cumulus convection and associated dynamic cloud processes like organized or turbulent en-/detrainment are often modeled by so-called “mass flux schemes”. While several studies (e. g., [37,38]) have stated the minor importance of convective clouds in the Arctic, Pinto and Curry [39], Curry *et al.* [40], and Rozwadowska and Cahalan [41] have shown that even over Arctic sea ice shallow convective clouds emanate from open water in leads or polynyas. Further, Sato *et al.* [42] have recently identified that these cumuliform clouds rather become more important in the Arctic due to the shift from ice-covered to ice-free Arctic ocean during autumn which can be associated with more well-mixed than stable ABL structures. Convective cloud processes are even important for stratiform cloud formation, such that, e. g., convective detrainment at the cloud top can be a direct source for stratiform cloud cover. To simulate stratiform clouds, current climate models commonly use complex bulk microphysics (e. g., [43,44]) and apply either relative humidity cloud schemes (RH-Schemes) or statistical cloud schemes as pointed out by Tompkins [45] or Zhu and Zuidema [46].

The motivation to this study was to evaluate and possibly adapt the subgrid-scale parameterization of Arctic clouds in the single-column climate model (SCM) HIRHAM5-SCM. SCMs are considered as a useful tool for developing and evaluating physical parameterizations of climate models, and thus have been exploited in various Arctic studies [47–50]. Here, the newly designed SCM version of the most recent RCM version HIRHAM5 [51] was exploited to analyze the two selectable cloud schemes for inner-Arctic climate conditions. The HIRHAM5-SCM setup and the applied cloud parameterizations are described in Section 2. Results of the model evaluation are presented and discussed in Section 3. In the first subsection, modeled height profiles of temperature and relative humidity as well as total cloud cover are validated against observations from NP-35 followed by some statistics. In the second subsection,

some cloud-related model variables are discussed with respect to their credibility. An evaluation of simulated cloudiness, using either the RH-Scheme by Sundquist *et al.* [52] or the prognostic statistical cloud scheme (PS-Scheme) by Tompkins [45], with two satellite-derived cloud data sets is shown afterwards. In Section 4 several model parameters are analyzed by means of sensitivity experiments for their potential to adapt the cloud parameterization to Arctic climate conditions. Finally, Section 5 contains conclusions and gives an outlook.

## 2. Model Description

### 2.1. HIRHAM5-SCM Setup

The employed SCM is based on the three-dimensional atmospheric RCM HIRHAM5 [51], which comprises the dynamical core of the regional weather forecast model HIRLAM (High Resolution Limited Area Model, [53]) and the physical parameterization package of the atmospheric general circulation model ECHAM5 (European Center Hamburg Model, [54]). HIRHAM5-SCM has 60 non-equidistant vertical levels, reaching from the surface up to a pressure height of 0.1 h, where the lowermost 1 km is represented by approximately 10 levels. The levels are given in hybrid  $\sigma$ - $p$ -coordinates following the ECMWF (European Center for Medium-Range Weather Forecasts) model level definitions by Berrisford *et al.* [55].

The hydrostatic model HIRHAM5 solves seven prognostic equations for the horizontal wind components  $u$  and  $v$ , temperature  $T$ , specific humidity  $q$ , cloud water content  $q_l$ , cloud ice content  $q_i$ , and surface pressure  $p_s$ . The total tendency of a prognostic variable can be split into a physical (diabatic) and a dynamical (adiabatic) part, where the former describes temporal changes due to subgrid-scale processes like radiation, cloud formation, and vertical diffusion. HIRHAM5-SCM calculates physical tendencies explicitly, using an explicit Euler forward time stepping scheme with 10 min time step. Since the dynamical part cannot be computed by a SCM, HIRHAM5-SCM uses prescribed  $p_s$  and dynamical tendencies of  $u$ ,  $v$ ,  $T$ , and  $q$  in all model levels.

Dynamical tendencies, as resulting mainly from advection, play a fundamental role in controlling the evolution of the model state. Bergman and Sardeshmukh [56] have demonstrated that the consideration of dynamical tendencies leads to a dynamic stabilization of SCMs, avoiding the drift into non-physical states. In this study, dynamical tendencies were extracted from the most recent ECMWF reanalysis data set “ERA-Interim” (see [57]). This reanalysis provides 3-hourly total and physical tendencies of  $u$ ,  $v$ ,  $T$ , and  $q$  for recalculating the dynamical tendencies. It should be noted that advection of  $q_l$  and  $q_i$  could not be considered, since corresponding ERA-Interim tendencies are not available. The treatment of dynamical tendencies was similar to the method of “revealed forcing” as introduced by Randall and Cripe [58], but a nudging technique as explained by Lohmann *et al.* [59] was not applied. Further, ERA-Interim data was used for prescribing  $p_s$  and the initialization of HIRHAM5-SCM.

The SCM-column was fixed in location during a single simulation, which always started at 0 UTC 1 August 2007 and mainly ran over 13 months to cover a whole annual cycle. In the present study, most of the model simulations were performed at the start coordinates of NP-35, which was located north of Severnaya Zemlya at 102.81°E longitude and 81.40°N latitude (figure with NP-35 track provided

at [60]). For comparing model results with individual observations from NP-35 (see Section 3.1) the SCM-column was set to the position of the NP-35 trajectory at the time of the respective measurement. This means that both the initial values and the prescribed  $p_s$  as well as dynamical tendencies were taken from the ERA-Interim grid point closest to the ice station at the time of the measurement. Since NP-35 measurements were carried out over a relatively large ice floe, all HIRHAM5-SCM runs used adapted, constant lower boundary conditions in terms of sea-ice fraction (100%), sea-ice thickness (2 m), and sea-surface temperature (271.38 K). The latter represents the freezing point of sea water and was only used for calculating the conductive heat flux through the 2 m thick sea-ice layer. The fixed 2 m thickness of the modeled ice floe represents a reasonable approximation to the ice thicknesses measured at NP-35.

## 2.2. Cloud Cover Parameterizations

Since the main focus of this study was on Arctic clouds and due to the strong interaction between cloud and radiation processes, a brief introduction into the radiation and cloud cover parameterizations is given in the following.

The applied ECHAM5 parameterization package contains a scheme for the SW and LW radiation transfer, respectively [54]. In the longwave, the “Rapid Radiative Transfer Model” (RRTM) radiation code is used, which is based on the two-stream approximation. Apart from two modifications, the SW radiation code is the same as in the previous model version ECHAM4 [61]. First, the number of spectral bands has been doubled from two to four (two additional bands in the near-infrared) to avoid spurious absorption in clouds [62]. Second, transmissivities and reflectivities are separately calculated for the cloud-free and cloudy part of a grid box.

The scheme for the representation of stratiform clouds consists of three components: (1) prognostic equations for the vapor, liquid, and ice phase; (2) cloud microphysics according to Lohmann and Roeckner [43]; and (3) the PS-Scheme developed by Tompkins [45]. As an option within the model, the cloud cover scheme of the previous ECHAM4 version [61] can be chosen alternatively. This scheme is a RH-Scheme as formulated by Sundquist *et al.* [52]. Cloud microphysics considers precipitation formation by coalescence processes, aggregation of ice crystals to snow flakes, and accretion of cloud droplets by falling snow, as well as processes like gravitational sedimentation of ice crystals, evaporation of rain and sublimation of snow and ice, and also freezing of cloud liquid water and melting of cloud ice. Furthermore, phase changes between the water components due to condensation/evaporation and deposition/sublimation are considered.

In the RH-Scheme, fractional cloud cover  $C$  is derived from the diagnostic relation

$$C = 1 - \sqrt{\frac{1 - \overline{\text{RH}}}{1 - \text{RH}_{\text{crit}}}} \quad (1)$$

where  $\overline{\text{RH}}$  represents the grid box mean and  $\text{RH}_{\text{crit}}$  the critical threshold of relative humidity. The latter decreases exponentially from 90% near the surface to 70% at higher altitudes (see [43]) and controls the onset of cloud formation.

In the PS-Scheme, subgrid-scale variability of total atmospheric water content  $q_t = q + q_c$  is explicitly specified by a probability density function (PDF) in terms of the beta distribution  $G(q_t)$ .

Note that  $q_c = q_l + q_i$  defines the cloud condensate as sum of cloud water and cloud ice content. The scheme includes prognostic equations for the higher order moments of the beta distribution, namely variance (distribution width) and skewness, which are linked to subgrid-scale processes like turbulence, convection, and microphysics (see [45]). Fractional cloud cover is then computed as integral over the supersaturation part ( $q_t > q_s$ ) of the actual beta distribution:

$$C = \int_{q_s}^b G(q_t) dq_t = 1 - I_x(\tilde{p}, \tilde{q}) \tag{2}$$

where  $b$  is the upper bound of  $G(q_t)$  and  $q_s$  denotes the saturation water content.  $I_x(\tilde{p}, \tilde{q})$  defines the ratio of incomplete to complete beta function, where  $x = (q_s - a)/(b - a)$  with the lower distribution bound  $a$ , and  $\tilde{p}$  and  $\tilde{q}$  are the shape parameters of the beta distribution. Following Tompkins [45], the shape parameter  $\tilde{p}$  is fixed in the model ( $\tilde{p} = 2$ ). In contrast,  $\tilde{q}$ , which is referred to as skewness parameter, is determined prognostically by

$$\frac{\partial \tilde{q}}{\partial t} = \left(\frac{\partial \tilde{q}}{\partial t}\right)_{\text{turb}} + \left(\frac{\partial \tilde{q}}{\partial t}\right)_{\text{conv}} + \left(\frac{\partial \tilde{q}}{\partial t}\right)_{\text{micro}} \tag{3}$$

where the terms on the right-hand side refer to temporal changes due to turbulence, convection, and microphysical processes, respectively.

Finally, the total cloud cover  $C^{\text{tot}}$  is calculated by the model using a maximum-random overlap assumption with respect to computed values of  $C$  in the respective model levels. Clouds in contiguous layers are maximally overlapped, while clouds separated by one or more clear-sky layers are randomly overlapped.

The PS-Scheme includes the two adjustment parameters  $\tilde{q}_0$  and  $K$ . The first parameter  $\tilde{q}_0$  determines the shape of the symmetric beta distribution and appears in the turbulence term of the skewness equation

$$\left(\frac{\partial \tilde{q}}{\partial t}\right)_{\text{turb}} = (\tilde{q}_0 - \tilde{q}) \left[ \frac{1}{\tau_v} + \frac{1}{\tau_h} \right] \tag{4}$$

Here,  $\tau_v$  and  $\tau_h$  denote the vertical and horizontal mixing time scales (see [45]). While  $\tau_v^{-1}$  depends on the mixing length and the turbulent kinetic energy,  $\tau_h^{-1}$  is neglected since horizontal mixing is not available in the SCM version. Turbulent mixing processes due to subgrid-scale eddies mainly lead to a reduction of skewness and, therefore, to an aspiration towards a symmetric beta distribution. Currently,  $\tilde{q}_0 = \tilde{p} = 2$  is used as default value, restricting the skewness of  $G(q_t)$  to a co-domain of  $[0, \sqrt{2})$ .

The second adjustment parameter  $K$ , which is set to the default value of  $K = 10$ , appears in the convection term of the skewness equation

$$\left(\frac{\partial \tilde{q}}{\partial t}\right)_{\text{conv}} = \frac{K}{\bar{\rho} q_s} \frac{\partial}{\partial z} (M^{\text{cu}} \bar{q}_c^{\text{cu}}) \tag{5}$$

and specifies how fast the skewness of the beta distribution increases according to the detrainment of cloud condensate due to cumulus convection. In Equation (5),  $\bar{\rho}$  is the mean air density and  $M^{\text{cu}} \bar{q}_c^{\text{cu}}$  represents the mass flux of cloud condensate due to convective updraft, where  $M^{\text{cu}}$  denotes the updraft mass flux and  $\bar{q}_c^{\text{cu}}$  the mean cloud condensate inside the updraft, assuming that  $\bar{q}_c^{\text{cu}} \gg \bar{q}_c$ . The superscript “cu” denotes that the respective variables are calculated by the cumulus convection scheme, which is

based on the mass flux scheme of Tiedtke [63] with modifications for penetrative convection according to Nordeng [64].

In addition, model parameters contained in the cloud microphysics were analyzed, since they have a direct influence on cloud formation and dissipation. One of these parameters is the minimum cloud water content  $CW_{\min}$ , which avoids negative  $q_l$  and  $q_i$ , and which is additionally a threshold for the existence of clouds in the PS-Scheme. If the grid box means of cloud liquid and cloud ice content fulfill  $\bar{q}_l \leq CW_{\min}$  and  $\bar{q}_i \leq CW_{\min}$ ,  $C$  will be set to zero. Thus, clouds will only appear in the PS-Scheme if at least one of the two variables exceeds  $CW_{\min}$ . The default value of  $0.1 \text{ mg kg}^{-1}$  was used in accordance to Zhang and Lohmann [49].

An overview on the modified model parameters is given in Table 1 (for equations and further details see Roeckner *et al.* [54]).

**Table 1.** Notation, default value, regarded parameter range (co-domain), and description of modified model tuning parameters. Apart from  $CW_{\min}$ , which is not mentioned by Roeckner *et al.* [54], the notation conforms to the ECHAM5 documentation.

Parameter	Default	Co-domain	Description (Meaning)
$\tilde{q}_0$	2	$1.00001 \leq \tilde{q}_0 \leq 20$	determines the shape of the symmetric beta distribution, which is used as PDF in the PS-Scheme
$K$	10	$0 \leq K \leq 10,000$	determines the efficiency of convective detrainment to increase the skewness of the beta distribution
$CW_{\min}$	$0.1 \text{ mg kg}^{-1}$	$(0 \leq CW_{\min} \leq 750) \text{ mg kg}^{-1}$	avoids negative cloud water and ice contents and additionally controls the occurrence of clear-sky conditions in the PS-Scheme
$\gamma_1$	15	$0 \leq \gamma_1 \leq 500$	determines the efficiency of rain drop formation by collision and coalescence of cloud drops (autoconversion rate)
$\gamma_2$	5	$0 \leq \gamma_2 \leq 50$	determines the efficiency of rain drop growth by collision and coalescence with cloud drops as well as the efficiency of snow flake growth by aggregation of surrounding ice particles
$\gamma_3$	95	$0 \leq \gamma_3 \leq 500$	determines the efficiency of snow formation by aggregation of cloud ice particles (aggregation rate)
$\gamma_4$	0.1	$0 \leq \gamma_4 \leq 100$	determines the accretion rate of ice crystals by supercooled cloud drops (growth of snow crystals) through colliding and coalescing with them (riming)
$\gamma_{\text{thr}}$	$0.5 \text{ mg kg}^{-1}$	$(0 \leq \gamma_{\text{thr}} \leq 5) \text{ mg kg}^{-1}$	cloud ice threshold, which determines the efficiency of the Bergeron–Findeisen process

### 3. Evaluation of Two Cloud Cover Schemes

#### 3.1. Evaluation with NP-35 Measurements

To evaluate the performance of HIRHAM5-SCM, a series of case studies was conducted, and then model results were compared with NP-35 measurements carried out from middle of October 2007 to the beginning of April 2008. For the comparison with an individual measurement, a single model run (from 0 UTC 1 August 2007 to the time of the measurement) was performed, respectively and during model start the SCM-column was set to the corresponding position of NP-35 according to Table 2 (as explained in Section 2.1). On the one hand, simulated vertical profiles of temperature  $T$  and relative humidity RH were checked against NP-35 radio soundings, which were started twice a day at 0 UTC and 12 UTC. On the other hand, modeled and observed total cloud cover  $C^{\text{tot}}$  were compared, where the latter was available from 6-hourly NP-35 weather reports.

Except for April 2008, where the first radio sounding was available on 2 April and the last available radiosonde was started on 7 April, the 1st and 15th of a respective month at midnight and midday were chosen for the evaluation (see Table 2). Exemplarily, Figure 1 shows observed and modeled height profiles of  $T$  and RH, and additionally modeled fractional cloud cover  $C$  at three specific events.

##### 3.1.1. Three Specific Cases

To illustrate the different performance of RH-Scheme and PS-Scheme, three cases associated with totally overcast (0 UTC 1 November 2007), clear-sky (12 UTC 15 January 2008), and partially cloudy (0 UTC 2 April 2008) conditions with respect to observed  $C^{\text{tot}}$  (see Table 2) were chosen.

**Table 2.** Listed are the geographic location (Longitude, Latitude) of the SCM-column for conducted case studies corresponding to the respective NP-35 radiosonde ascent and both observed and modeled total cloud cover  $C^{\text{tot}}$  using either the PS-Scheme or RH-Scheme. In the notation “yyyy-mm-dd\_hh”, “yyyy” = year, “mm” = month, “dd” = day and “hh” = hour. Dates in bold type are discussed in detail in Section 3.1.1.

Date	Lon (°E)	Lat (°N)	$C^{\text{tot}}$ (%)		
			NP-35	SCM(PS)	SCM(RH)
2007-10-15_00	101.86	81.60	100.0	89.6	100.0
10-15_12	102.22	81.56	100.0	100.0	100.0
<b>11-01_00</b>	<b>102.06</b>	<b>82.42</b>	<b>100.0</b>	<b>100.0</b>	<b>100.0</b>
11-01_12	101.86	82.40	0.0	64.6	100.0
11-15_00	97.52	82.10	0.0	0.0	0.0
11-15_12	97.55	82.11	0.0	100.0	100.0
12-01_00	97.56	83.02	0.0	100.0	100.0
12-01_12	97.31	82.99	100.0	100.0	100.0
12-15_00	97.69	83.40	0.0	0.0	0.0
12-15_12	97.92	83.45	0.0	0.0	0.0
2008-01-01_00	92.49	84.75	0.0	0.0	100.0
01-01_12	92.32	84.73	0.0	0.0	0.0
01-15_00	91.82	85.06	0.0	100.0	100.0

**Table 2.** *Cont.*

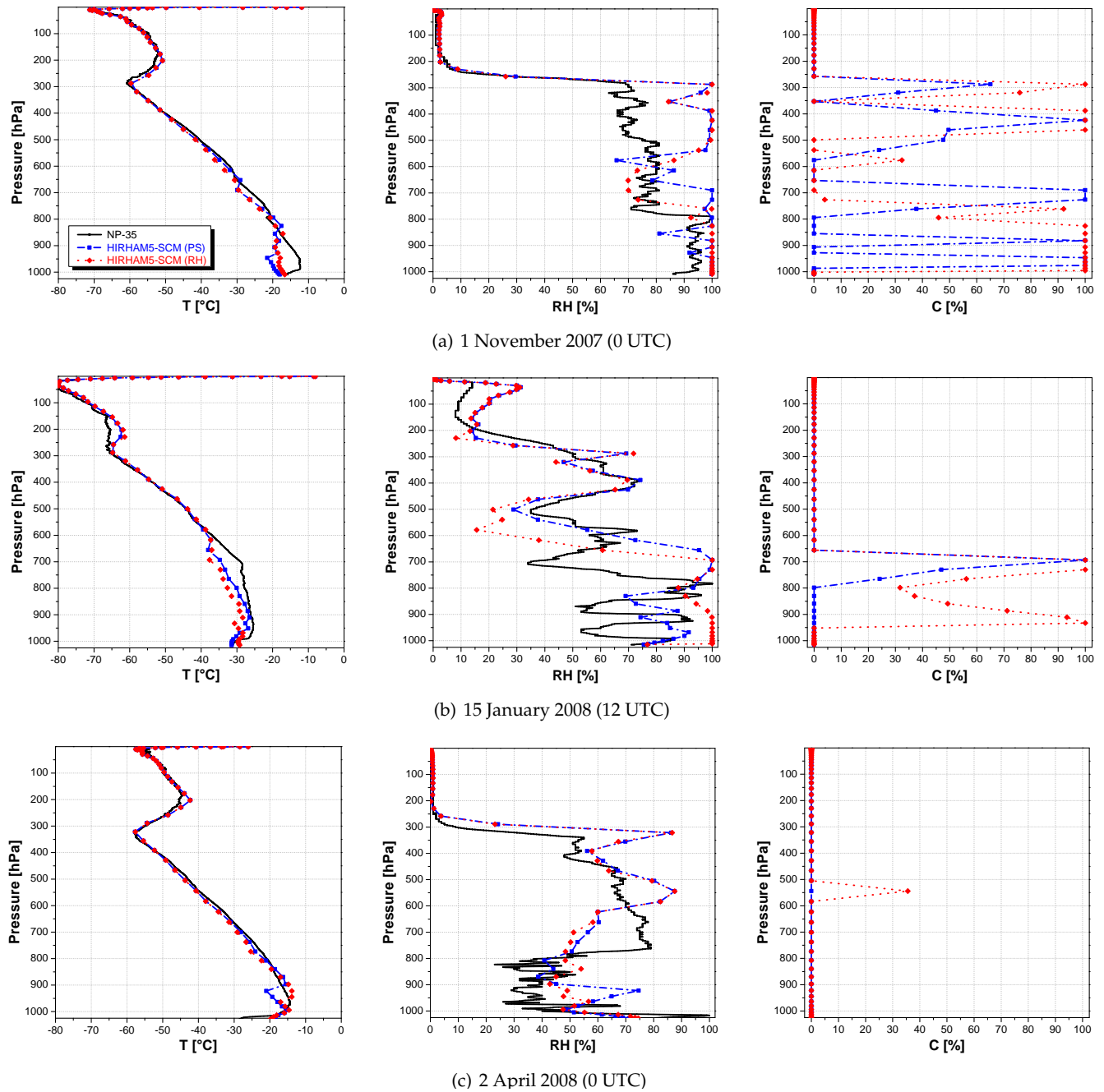
Date	Lon (°E)	Lat (°N)	$C^{\text{tot}}$ (%)		
			NP-35	SCM(PS)	SCM(RH)
<b>01-15_12</b>	<b>91.13</b>	<b>85.04</b>	<b>0.0</b>	<b>100.0</b>	<b>100.0</b>
02-01_00	78.12	85.17	0.0	100.0	100.0
02-01_12	77.98	85.15	100.0	100.0	100.0
02-15_00	71.51	85.65	100.0	100.0	84.9
02-15_12	71.31	85.64	100.0	0.0	0.0
03-01_00	61.16	85.52	100.0	58.1	79.8
03-01_12	60.97	85.50	0.0	0.0	0.0
03-15_00	55.96	85.52	0.0	0.0	100.0
03-15_12	60.98	85.50	25.0	0.0	0.0
<b>04-02_00</b>	<b>42.23</b>	<b>84.75</b>	<b>87.5</b>	<b>0.0</b>	<b>45.8</b>
04-02_12	42.22	84.71	12.5	15.0	0.0
04-07_00	42.21	84.29	100.0	0.0	0.0
04-07_12	41.90	84.27	0.0	0.0	0.0

Figure 1(a) reveals high  $C$  on 1 November 2007 independent from the used cloud scheme, where low- (below 700 h), mid- (700 to 400 h), and high-level (above 400 h) clouds were simulated. While the RH-Scheme produced a totally overcast sky below 810 h, the PS-Scheme showed pressure ranges with alternating clear-sky and overcast conditions. In the middle troposphere the PS-Scheme simulated an overcast sky around 710 h, whereas the RH-Scheme produced one low-level and mid-level cloud layer around 761 h and 576 h, respectively associated with partial cloudiness. The vertical cloud structures were very similar above 500 h, but the RH-Scheme simulated up to 35% higher absolute values. On 1 November 2007 polar night has already prevailed (at current NP-35 position, see Table 2) so that Arctic clouds can be associated with near-surface warming independent from cloud family due to the absence of SW CRF. Thus, the enhanced cloudiness simulated by the RH-Scheme leads to higher temperatures in the near-surface layer and allows for a better match to the observation, which is confirmed by near-surface temperature differences of  $-2.3$  K (PS-Scheme) and  $-0.8$  K (RH-Scheme), respectively. On the other hand, the PS-Scheme is better able to model the linkage between the occurrence of Arctic stratus clouds and capping strong temperature inversion as well as rapid moisture decrease (e. g., 882 to 855 h). Nevertheless, this linkage does not always agree with the observation (e. g., 690 to 653 h). In agreement with the NP-35 observation both cloud schemes produced a  $C^{\text{tot}}$  of 100% (*cf.* Table 2).

On 15 January 2008 (Figure 1(b)) the RH-Scheme produced two overcast cloud decks around 933 h and 693 h, respectively with partially cloudy conditions in between. In contrast, the PS-Scheme simulated only the upper-level cloud deck. While the PS-Scheme matches the observed RH-profile much better between 450 to 610 h and from 800 h to the surface, modeled profiles of RH are almost identical and in part accurately agree with the measurement (e. g., 360 to 440 h). The RH-Scheme overestimates measured RH significantly (up to 47%) from 1,012 h to 830 h, leading to more BLCs associated with enhanced LW CRF and 2.2 K higher near-surface temperatures relative to the PS-Scheme. Although both cloud schemes consistently produced low-level clouds and also the same  $C^{\text{tot}}$  of 100%, this totally differs from the observed clear sky. Since the PS-Scheme simulated less clouds below 600 h, it likely

matches the observed  $T$ -profile better in the ABL, but the actual temperature structure is of course also determined by other processes like turbulent vertical heat exchange and cannot be explained only by the effect of CRF.

**Figure 1.** Vertical profiles of temperature  $T$  (in  $^{\circ}\text{C}$ ) (*left column*), relative humidity RH (in %) (*middle column*), and fractional cloud cover  $C$  (in %) (*right column*) at various dates, originating from NP-35 radiosonde ascents (*black curves*) and HIRHAM5-SCM simulations using either the PS-Scheme (*blue curves*) or RH-Scheme (*red curves*).



Contrary to the cases before, on 2 April 2008 (Figure 1(c)) only the RH-Scheme produced fractional cloud cover around 544 h, while both modeled RH-profiles were almost identical here and also above. Overall, the RH-Scheme produced a  $C^{\text{tot}}$  of 45.8% implying a much smaller difference (41.7%) to the

observed NP-35 value. Significant differences between the two simulated profiles of RH occurred in the pressure range from 623 h to 964 h, where the PS-Scheme agrees better with the NP-35 observation between 623 to 897 h but worse between 897 to 964 h. The two modeled temperature structures were very similar above 897 h matching the observation fairly well. Although the RH-Scheme simulated some mid-level clouds, the measured strong ground-based temperature inversion is underestimated as by the PS-Scheme (about 9 K too warm inversion base). Partial cloudiness produced by the RH-Scheme improves the simulated temperature profile between 897 to 964 h, but the consistently modeled elevated temperature inversion starting in 963 h (RH-Scheme) and 922 h (PS-Scheme), respectively totally disagrees with the measurement. The NP-35 radiosonde ascent showed 100% RH around 1,016 h and low near-surface temperatures of  $-28.7^{\circ}\text{C}$  arguing for a low-level cloud deck associated with dominant SW CRF (enhanced cloud albedo effect), which could not be reproduced by the model.

Wang *et al.* [65] have demonstrated that the surface temperature is higher in the presence of multi-layered Arctic clouds than in cases of single-layer BLCs. This finding is in accordance to Figure 1(b). LW radiative cooling at the cloud top generates energetic turbulent eddies which effectively transport the radiatively cooled air down to the ground, except for the storm-driven cloudy ABL [29]. This effect is most likely overestimated by the model (as suggested in Figure 1(a,b)) favoring condensation or resublimation which finally leads to enhanced cloud formation. While deviations between modeled  $T$ - and RH-profiles are generally small in case of similar cloud profiles, they become significant as soon as the two cloud schemes simulate different vertical cloud structures. Although both cloud schemes sometimes model almost the same  $T$ - and RH-profiles, they can significantly differ from the observation especially in the ABL. Even when complete absence of model clouds is consistently produced in the entire SCM-column (not shown), simulated  $T$ - and RH-profiles either can differ from each other or do not agree with the observation. In general, the more pronounced vertical variability of moisture cannot be reproduced accurately by the model. Thus, the RH-Scheme a priori produces clouds at incorrect altitudes.

### 3.1.2. Statistics over All Cases

To validate simulated profiles of  $T$  and RH quantitatively for the 26 studied cases, the Pearson product-moment correlation (autocorrelation) coefficient  $r$  was computed in every model level with respect to NP-35 measurements. Since none of the studied NP-35 radiosondes rose higher than 7 h and at least two radiosonde measurements should be available for a certain pressure height,  $r$  could only be calculated for the 48 uppermost model levels (lowermost altitudes), where the 13th model level is situated in about 8 h (32 km height).

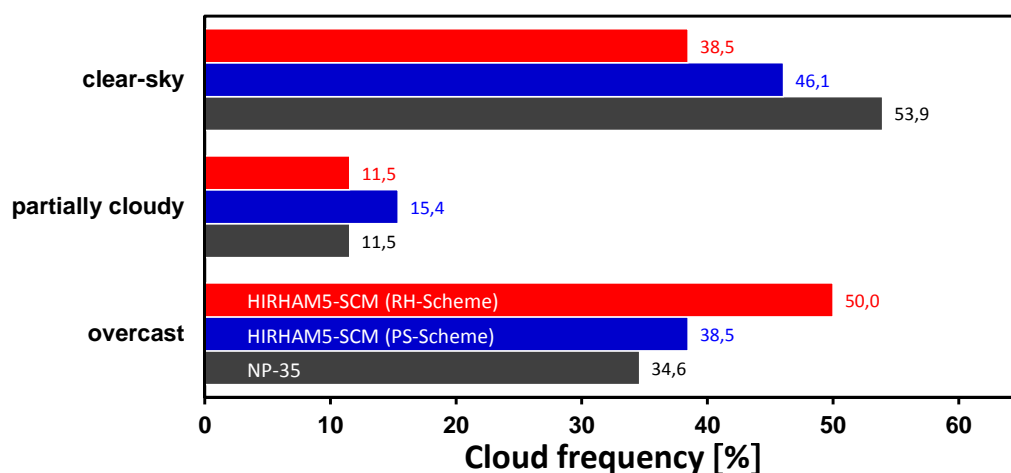
For temperature, solely positive and high correlation coefficients ( $r_T > 0.75$ ) were calculated within the entire atmospheric column independently from the applied cloud scheme. While the temperature correlation was consistently very high ( $>0.99$ ) above the 30th model level (about 200 h), the strength of the linear relation decreased below and became minimal in the ABL. This was confirmed by vertically averaged correlation coefficients  $\hat{r}_T$  computed either for the entire SCM-column or the 10 model levels closest to the surface. While the PS-Scheme produced  $\hat{r}_T = 0.95$  (13 to 60 model level) and  $\hat{r}_T = 0.86$  (51 to 60 model level), the RH-Scheme showed slightly lower mean correlations of 0.94 and 0.85, respectively. HIRHAM5-SCM generally produced comparably low temperature correlations in

the three model levels closest to the surface ( $r_T < 0.85$  for RH-Scheme) indicating incorrect turbulent heat fluxes. Interestingly, lowest values of  $r_T$  (up to 0.76) appeared around the 52nd model level (about 930 h), which might be explained with an incorrect coupling between ABL and the free troposphere in the model. The RH-Scheme produced slightly higher correlation coefficients between the 51st (about 910 h) and 54th (about 965 h) model level but otherwise the PS-Scheme produced either equal or higher correlations. Overall, the PS-Scheme therefore correlates better with measured NP-35 profiles of  $T$ .

Correlation coefficients of relative humidity were mainly high ( $r_{RH} > 0.75$ ) above the 38th model level (about 460 h). As compared with  $r_T$  the correlation coefficients of RH were also positive but decreased faster with increasing model level (decreasing altitude) and rarely dropped below 0.4 up to the 56th model level (around 990 h). In contrast, the four model levels closest to the surface were associated with low correlation coefficients ( $|r_{RH}| < 0.3$ ) and were even negative in case of the RH-Scheme. Negative correlation coefficients in the near-surface layer indicate more serious problems in correctly simulating ground-based temperature inversions leading to incorrect vertical moisture fluxes. The vertically averaged correlation coefficients  $\hat{r}_{RH}$  with respect to the entire atmospheric column (0.70 and 0.68 for PS-Scheme and RH-Scheme, respectively) and the ABL (0.33 and 0.29 for PS-Scheme and RH-Scheme, respectively) confirmed that the model has more serious difficulties in accurately simulating the ABL, but also that the PS-Scheme correlates better with measured NP-35 profiles of RH.

For further validating the applied cloud schemes against NP-35, relative frequencies of clear-sky, partially cloudy, and (totally) overcast cases were calculated. Figure 2 reveals that clear-sky conditions prevailed in more than half the observations, slightly more than one third represented overcast conditions, and only in slightly more than one ninth of the cases partial cloudiness was observed.

**Figure 2.** Relative frequencies of clear-sky, partially cloudy, and overcast cases based on all 26 conducted case studies (Table 2), shown for NP-35 observations and model simulations using either the PS-Scheme or RH-Scheme.



On the one hand, the RH-Scheme agrees with the observed frequency of partially cloudy cases (11.5%), while about 4% more cases are produced by the PS-Scheme. On the other hand, the model underestimates clear-sky cases by 7.8% (PS-Scheme) and 15.4% (RH-Scheme) but overestimates overcast cases by 3.9% (PS-Scheme) and 15.4% (RH-Scheme). Overall, HIRHAM5-SCM overestimates cloudy cases (sum of partially cloudy and overcast cases) by the same percentages as for the

underestimation of clear-sky cases and therefore, the PS-Scheme matches NP-35 observations much better.

### 3.2. Arctic Clouds in the Reference Run

Starting point for the sensitivity studies in Section 4 was a reference run that uses the standard configuration of the model (usage of default model parameters). Here, a single HIRHAM5-SCM reference run (from 1 August 2007 to 31 August 2008) was conducted for both the PS-Scheme and RH-Scheme.

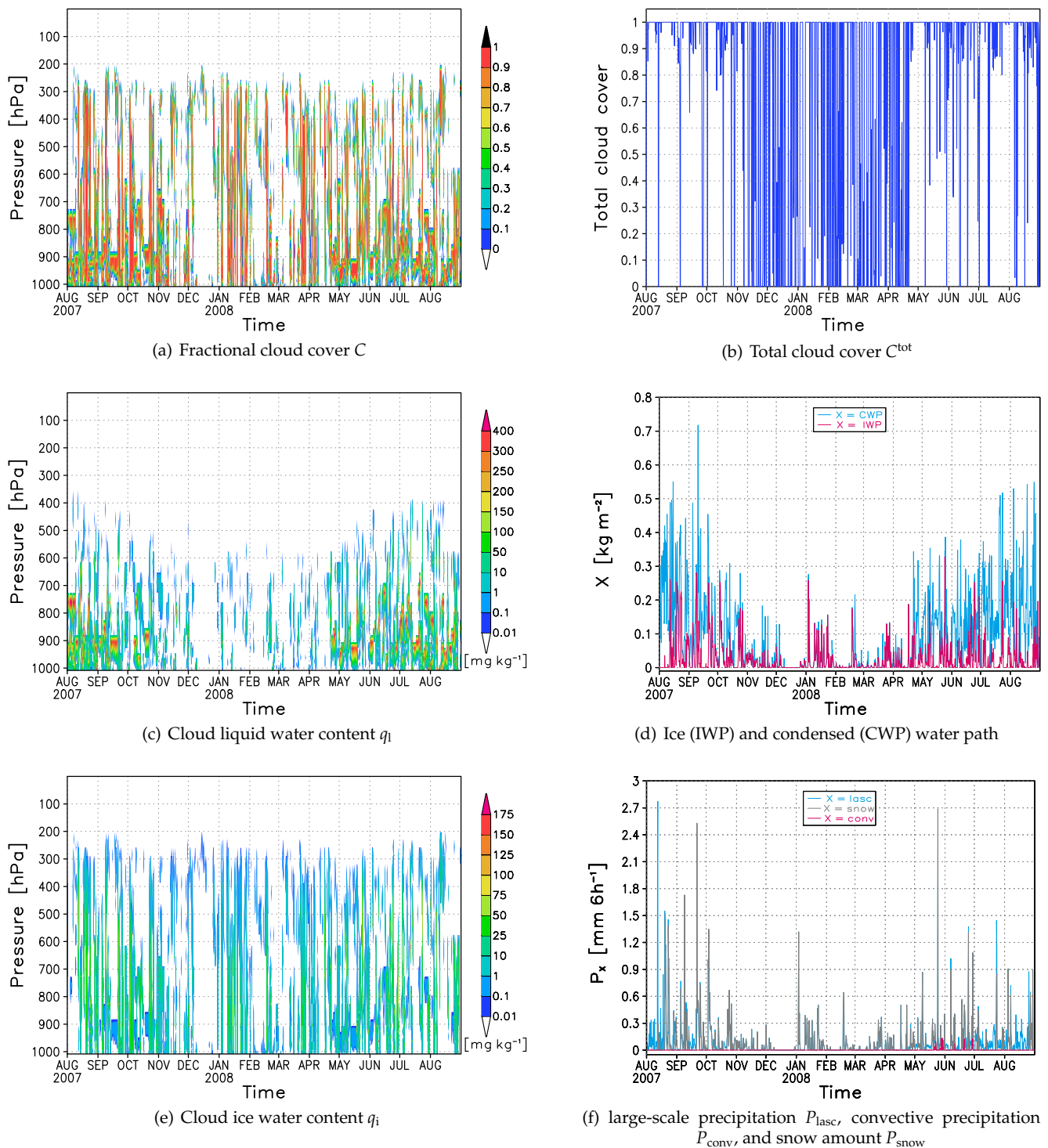
#### 3.2.1. Annual Cycle of Cloud-Related Variables

Applying the PS-Scheme, Figure 3 shows time-height cross sections of  $C$ ,  $q_l$ , and  $q_i$  as well as the temporal evolution of  $C^{\text{tot}}$ , ice water path IWP, condensed water path CWP (sum of liquid and ice water paths), large-scale (stratiform)  $P_{\text{las}}c$  and convective  $P_{\text{conv}}$  precipitation, and additionally the snow amount  $P_{\text{snow}}$  with respect to total precipitation  $P^{\text{tot}} = P_{\text{las}}c + P_{\text{conv}}$ .

Figure 3(a,b) reveal rather moderate cloudiness during the WP (winter period: from mid-November 2007 to mid-April 2008; *i.e.*, predominantly polar night) associated with strong fluctuations between (totally) overcast (49.7%) and clear-sky (31.6%) conditions. On the other hand, the PS-Scheme produced enhanced cloudiness during the SP (summer period: entire modeled time range except for WP; *i.e.*, predominantly polar day), where an overcast sky (75.3%) occurred more often than a clear sky (5.0%). In particular, low-level clouds (below 700 h) appeared more often during summer and autumn in accordance to the frequently observed presence of summertime BLCs (e. g., [14]). Inoue *et al.* [29] have found one possible mechanism for the layered structure of summertime BLCs, which depends on the combination of shear mixing near the surface and radiative cooling at the cloud top in the storm-driven cloudy ABL. The RH-Scheme behaved similar during the SP (not shown), but overall, this cloud scheme tends to simulate larger cloud amounts in general (confirmed by Section 3.2.2). In fact, during the SP an overcast sky (77.4%) occurred also more often than a clear sky (4.7%), while the RH-Scheme produced much more cases with overcast conditions (about 10% more than PS-Scheme) but less cases with clear-sky conditions (about 3% less than PS-Scheme) during the WP. The latter is basically the same result as obtained from the comparison with NP-35 (see Section 3.1.2).

In the PS-Scheme subgrid-scale sources and sinks of clouds directly control the temporal evolution of the cloud representing area below the beta distribution (see Section 2.2), and thus more realistic model cloudiness can be achieved as demonstrated by Tompkins [45]. An advanced feature is therefore the ability to simulate abrupt changes from totally overcast to clear-sky conditions (e. g., between 0 UTC and 6 UTC 13 August 2007 in Figure 3(b)) and *vice versa* (e. g., between 12 UTC and 18 UTC 13 August 2007 in Figure 3(b)), which were also apparent in NP-35 weather reports (not shown). The simulation of such abrupt changes in  $C^{\text{tot}}$  happened less often and rather randomly when using the RH-Scheme, because the subgrid-scale variability of water vapor is only indirectly considered by the threshold of relative humidity, and the linkage to cloud formation and dissipation processes is missing.

**Figure 3.** Simulated fractional (a) and total (b) cloud cover, cloud liquid (c) and ice (e) water content, ice and condensed (sum of liquid and ice water paths) water path (d) as well as large-scale and convective precipitation and the contribution of snow (f) for the period from 1 August 2007 to 31 August 2008. This HIRHAM5-SCM reference run was conducted at the NP-35 start position (102.81°E, 81.40°N) using the PS-Scheme and applying default model parameters (see Table 1). The results are shown as 6-hourly standard model output.



HIRHAM5-SCM produced a reasonable annual cycle of LWP, IWP, CWP, and  $P^{tot}$ . In accordance to Intrieri *et al.* [15] Figure 3(c,e) show the more often occurrence of ice-only clouds during the WP

than during the SP. While most of the simulated  $q_l$  was located below 700 h, significant amounts of  $q_i$  were still modeled above 500 h. Figure 3(d) reveals that wintertime Arctic mixed-phase clouds can be associated with lower LWPs compared to mixed-phase clouds of the SP, which agrees with findings of Shupe and Intrieri [3]. Simulated LWP and IWP had also the correct order of magnitude (e.g., [28]).  $P^{\text{tot}}$  was dominated by  $P_{\text{asc}}$  except for June and July 2008, where  $P_{\text{conv}}$  was generated as well (Figure 3(f)). During the SP much higher  $P^{\text{tot}}$  was modeled than during the WP, where the latter period was more dominated by  $P_{\text{snow}}$ .

Lohmann *et al.* [66] have shown that the stand-alone ECHAM5 GCM overestimates  $q_l$  (LWP) but underestimates  $q_i$  (IWP), and they have found an overestimation of  $q_c$  (CWP) as well as  $P^{\text{tot}}$ . Microphysical cloud characteristics from NP-35 are not available. Hence, these findings were qualitatively examined by comparison with observations carried out during the Surface Heat Budget of the Arctic Ocean (SHEBA, October 1997–1998). Our results (not shown) suggested a similar behavior in HIRHAM5-SCM as mentioned by Lohmann *et al.* [66].

### 3.2.2. Evaluation with Satellite Observations

On the one hand, the advanced International Satellite Cloud Climatology Project data set ISCCP-D2 [67] was used to evaluate the simulated monthly averaged  $C^{\text{tot}}$ . ISCCP-D2 cloud data refer to an equal-area grid with horizontal resolution of about 280 km and is provided at [68]. The second satellite-based data set originated from the Moderate Resolution Imaging Spectroradiometer (MODIS) “MOD08\_M3-Level3 Monthly Joint Aerosol Vapor/Cloud Product” described by Hubanks *et al.* [69]. This “Terra Atmosphere Level 3 Product” (Collection 5; [70]) provides a horizontal resolution of  $1^\circ \times 1^\circ$  (about 100 km). From both data sets the observed cloud amount was extracted from August 2007 to August 2008. While ISCCP-D2 cloud amount corresponded to grid center coordinates of  $106.36^\circ\text{E}$  and  $81.25^\circ\text{N}$ , MODIS cloud amount was used with respect to a longitude of  $103.0^\circ\text{E}$  and latitude of  $81.0^\circ\text{N}$ , being the nearest-neighbor grid points to the start coordinates of NP-35 ( $102.81^\circ\text{E}$ ,  $81.40^\circ\text{N}$ ).

First, Figure 4 reveals a qualitative disagreement between the annual cycles of ISCCP-D2 and MODIS, which was quantitatively confirmed by a relatively large overall root mean square error (RMSE of all 13 months) of 17.5% listed in Table 3. MODIS featured enhanced cloudiness ( $>70\%$ ) in the summer months and September but moderate cloudiness (fluctuating between 66.7% in January and 43.0% in March) during the rest of the year associated with distinct transitions starting in August 2007 and May 2008. This typical annual cycle of Arctic cloud cover has also been found in the satellite-based TOVS Polar Pathfinder data set ([71], not available after 2005) and ground-based observations by Hahn *et al.* [72]. In comparison to MODIS, ISCCP-D2 featured much more cloud cover from December to March (more than 30% higher in February) and less cloud cover during the rest of the year (more than 22% lower in August 2008), except for October. This leads to a reverse annual cycle in general, shifting the transition’s onsets to October (starting increase) and January (starting decrease). Apart from systematic and significant differences during the December–January–February season (highest RMSE of 23.8%) and March both satellite data sets at least produced same trends during the rest of the year. Further, ISCCP-D2 and MODIS agreed better during the summer period (SP) than during the winter period (WP), and the best statistical agreement appeared in the September–October–November season (lowest RMSE of 8.5%).

**Figure 4.** Monthly means of total cloud cover  $C^{tot}$  (in %) from August 2007 to August 2008 referring to the NP-35 start position. The results originate from both ISCCP-D2 (short dashed black line) and MODIS (solid black line) satellite observations, and HIRHAM5-SCM simulations using either the PS-Scheme (blue line) or the RH-Scheme (red line).

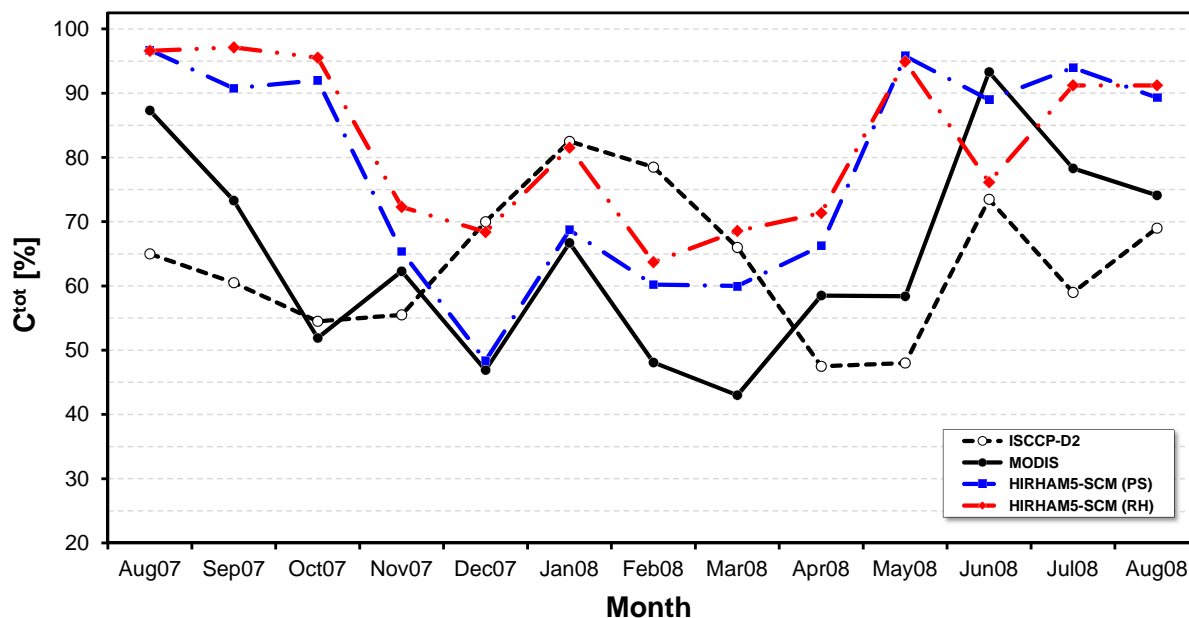


**Table 3.** Root mean square errors (RMSEs) of monthly averaged  $C^{tot}$  (in %) (based on Figure 4) for the satellite data sets among each other and in comparison with the HIRHAM5-SCM reference simulation using either the PS-Scheme or RH-Scheme.

		RMSE (%)			
		ISCCP-D2	MODIS	SCM (PS-Scheme)	SCM (RH-Scheme)
SON	ISCCP-D2	—	8.5	28.4	33.2
	MODIS	8.5	—	25.3	29.3
DJF	ISCCP-D2	—	23.8	18.2	8.6
	MODIS	23.8	—	7.1	17.6
MAM	ISCCP-D2	—	15.9	29.8	30.4
	MODIS	15.9	—	24.1	26.8
JJA	ISCCP-D2	—	16.2	25.0	22.6
	MODIS	16.2	—	12.9	15.9
WP	ISCCP-D2	—	20.0	15.7	13.4
	MODIS	20.0	—	9.2	17.5
SP	ISCCP-D2	—	15.0	32.7	33.3
	MODIS	15.0	—	23.6	25.8
all months	ISCCP-D2	—	17.5	26.3	26.1
	MODIS	17.5	—	18.4	22.3

In accordance to the present study for 2007/2008, Schweiger *et al.* [71] have figured out that the ISCCP-D2 climatological data set produces a reverse annual cycle of Arctic cloud cover as compared to ground-based and TOVS observations. They have demonstrated that ISCCP-D2 is associated with a systematic overestimation of Arctic clouds during polar night and underestimation during polar day. The advantages and disadvantages of ground-based and satellite-based cloud observations as well as their potential errors have been addressed e. g., by Eastman and Warren [18]. Wielicki and Parker [73] have shown that the detected cloud amount depends on the applied algorithm as well as on the spatial resolution of the used satellite sensor. The study of Schweiger *et al.* [71] and lower horizontal resolution of the ISCCP-D2 data set are indicative of larger credibility to MODIS.

HIRHAM5-SCM is qualitatively able to reproduce the annual cycle of Arctic cloud cover detected by MODIS regardless of the applied cloud scheme. Nevertheless, the model overestimates  $C^{\text{tot}}$  in most of the months, especially from May to October, when overcast conditions were modeled frequently as noted previously. This overestimation is on average slight but significantly larger when using the RH-Scheme (4% higher overall RMSE). Overall, the PS-Scheme matches MODIS observations better, where the WP shows better agreement than the SP (Table 3). From a seasonal point of view, the best agreement appeared between the PS-Scheme and MODIS during the DJF season. This good agreement is significantly reduced (by 10.1%) when the RH-Scheme is used. Furthermore, the model generally simulates Arctic clouds adequately during the JJA season. In contrast, the model overestimates both the decrease (SON) and increase (MAM) in Arctic cloud cover during the transition seasons. In comparison to MODIS the strongest decrease (between September and October 2007) and increase (between May and June 2008) in cloud cover tends to be shifted one month forward and backward respectively in the model. This leads to the most pronounced overestimations in October 2007 and May 2008, where the  $C^{\text{tot}}$  simulated by the PS-Scheme was 40.1% and 37.4% too high, respectively.

ABL processes should be considered as one possible source for deviations in cloud simulations. Zhao and Wang [74] have figured out that low-level cloud formation and maintenance mechanisms as well as cloud microphysical characteristics closely interact with ABL processes and are related to the ABL structure. The model's ability to adequately simulate Arctic clouds depends on the used ABL parameterization as shown by Axelsson *et al.* [75]. In our model, the interaction between clouds and turbulence is represented by processes such as the vertical exchange of turbulent kinetic energy (TKE) generated by radiative cooling at cloud top, the impact of cloud condensate on the buoyancy flux, and cloud top entrainment through the turbulent flux of cloud condensate.

In October 2007, through overestimated vertical mixing (biased simulation of ground-based temperature inversions, see Figure 1(a)), warmer moist air could be transported towards the colder lower model levels (cooled by enhanced cloud top radiative cooling) possibly enabling condensation or resublimation. Therefore, existing clouds likely either persisted or grew further, partially explaining the high overestimation of  $C^{\text{tot}}$ . During May 2008, also the upper model levels became gradually moister due to the simulated large turbulent moisture transports which most likely favored cloud formation under colder environmental conditions. The Arctic transition seasons are associated with distinct transitions in atmospheric conditions, e. g., in SW radiation fluxes, in sea ice (e. g., formation of leads or melt ponds), or changing horizontal moisture and aerosol transports from mid-latitudes. Arctic clouds are impacted

by such transitions which are difficult to realistically simulate, and therefore the model shows here the most pronounced biases.

Zhang and Lohmann [49] have studied Arctic spring cloud properties observed during the SHEBA project, and have compared the performance of the RH-Scheme used here with a statistical cloud scheme with positive but constant skewness. In accordance to our study, they have found that the statistical cloud scheme produces less cloud cover than the RH-Scheme. Based on ground-based radar cloud observations carried out in April 1998 they have concluded that the RH-Scheme agrees better with SHEBA observations during this single month. Here, a contrary behavior was found since Figure 4 confirms the better agreement between PS-Scheme and MODIS during April 2008, which can most likely be attributed to the more sophisticated statistical cloud scheme used in our study.

In conclusion, the PS-Scheme leads to an improved simulation of Arctic clouds as compared to the RH-Scheme, but the current formulation is far from being satisfactory due to the systematic overestimation of Arctic cloud cover. Tompkins [45] has already mentioned that his PS-Scheme results in an almost global improvement in the simulation of clouds, but with the possible exception of polar regions. The recently published study by Weber *et al.* [76], who have evaluated the PS-Scheme in ECHAM5 globally against MODIS, also identifies the systematic overestimation of  $C^{\text{tot}}$  in high latitudes.

#### 4. Parameter Sensitivity Studies

Sensitivity studies were conducted to assess the effect of modified model adjustment parameters (listed in Table 1) on cloud-related variables relative to the reference run (see Figure 3). One of the main goals was to identify suitable tuning parameters, which are potentially able to reduce the systematic overestimation of Arctic clouds in HIRHAM5-SCM. While the values of PS-Scheme tuning parameters are originally based on cloud resolving model simulations, tunable parameters of the cloud microphysics have been estimated by detailed microphysical models. These “tuning” parameters obviously need to be adapted for the usage in large-scale models as stated by Tompkins [45] and Roeckner *et al.* [54]. Further adjustment of these parameters is likely required again when changing from the global to the regional scale, thus necessitating our sensitivity experiments.

Each sensitivity experiment comprised a simulation over 13 months by analogy to the reference run but using a modified value of a single model parameter. Although every tuning parameter was varied within a certain parameter range (see Table 1), the following discussions will basically be restricted to one lower and higher value, respectively, since the main conclusions remain unchanged. Based on the simulations, differences between respective sensitivity run (hereinafter “SENS”) and reference run (hereinafter “CTRL”) were computed, and zero-cases were neglected. To quantify the impact of a certain parameter change, relative frequencies of “positive differences” ( $(\text{SENS} - \text{CTRL}) > 0$ ) were calculated for several cloud-related model variables both with respect to all 13 simulated months and the periods with moderate (WP) and high (SP)  $C^{\text{tot}}$  in the reference run. Let  $f$  be the relative frequency of positive differences, then the percental decrease ( $\Delta f < 0$ ) or increase ( $\Delta f > 0$ ) of a certain model variable relative to the reference run can be computed using the formula  $\Delta f = f - (100\% - f)$ . The results are listed in Tables 4 and 5 either with respect to *lower* or *higher* tuning parameters.

**Table 4.** Percental decrease/increase of several model variables due to *lower* parameter values ( $\tilde{q}_0 = 1.5$ ,  $K = 1$ ,  $CW_{\min} = 7.5 \times 10^{-4} \text{ mg kg}^{-1}$ ,  $\gamma_1 = 5$ ,  $\gamma_2 = 2$ ,  $\gamma_3 = 25$ ,  $\gamma_4 = 0.025$ ,  $\gamma_{\text{thr}} = 0.05 \text{ mg kg}^{-1}$ ) relative to the default (Table 1) for the entire 13-month-long simulations (“all”) as well as the winter (WP) and summer (SP) periods as introduced in Section 3.2.1.

		$\tilde{q}_0$	$K$	$CW_{\min}$	$\gamma_1$	$\gamma_2$	$\gamma_3$	$\gamma_4$	$\gamma_{\text{thr}}$
LWP	WP	18	16	1	16	14	11	14	-39
	SP	1	4	-12	33	9	-9	8	-41
	all	6	8	-9	28	10	-4	10	-41
IWP	WP	26	23	27	33	26	45	30	30
	SP	17	17	14	14	22	38	15	25
	all	20	20	18	21	23	40	20	25
CWP	WP	23	18	17	27	17	34	21	3
	SP	1	4	-16	30	10	3	7	-39
	all	8	9	-4	29	12	13	12	-25
$C^{\text{tot}}$	WP	-7	6	27	17	15	24	17	4
	SP	-27	9	-14	19	5	-6	2	-9
	all	-18	8	6	18	10	7	8	-4
$P_{\text{Iasc}}$	WP	16	19	25	27	16	23	20	17
	SP	-7	-1	-5	-6	-3	-2	2	3
	all	2	7	6	6	4	7	8	8
$P_{\text{conv}}$	WP	—	—	—	—	—	—	—	—
	SP	4	36	2	-18	18	-16	15	6
	all	4	36	2	-18	18	-16	15	6
$P_{\text{snow}}$	WP	17	20	26	27	16	22	21	17
	SP	14	18	22	28	21	24	16	34
	all	15	19	23	28	19	23	18	28

**Table 5.** Same as Table 4 but for *higher* parameter values ( $\tilde{q}_0 = 20$ ,  $K = 100$ ,  $CW_{\min} = 250 \text{ mg kg}^{-1}$ ,  $\gamma_1 = 100$ ,  $\gamma_2 = 8$ ,  $\gamma_3 = 200$ ,  $\gamma_4 = 10$ ,  $\gamma_{\text{thr}} = 1 \text{ mg kg}^{-1}$ ).

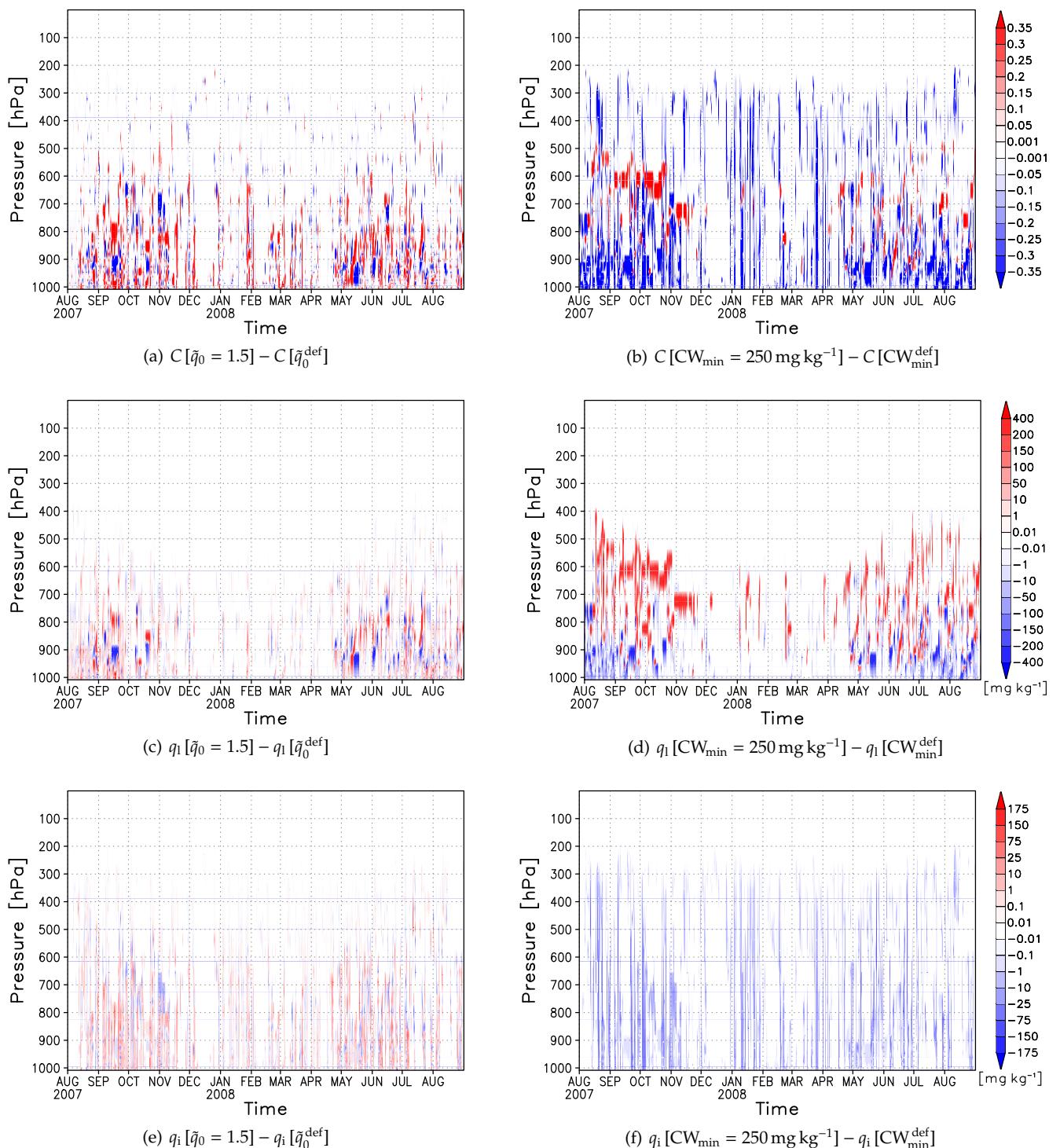
		$\tilde{q}_0$	$K$	$CW_{\min}$	$\gamma_1$	$\gamma_2$	$\gamma_3$	$\gamma_4$	$\gamma_{\text{thr}}$
LWP	WP	14	15	-12	18	15	6	-15	30
	SP	-9	-3	11	-44	-15	-3	-31	21
	all	-3	2	5	-27	-7	-1	-27	23
IWP	WP	23	31	-72	25	28	0	16	29
	SP	6	10	-85	-5	-4	-21	-18	1
	all	12	18	-80	6	8	-13	-6	11
CWP	WP	19	29	-42	20	22	-1	3	31
	SP	-10	-3	2	-45	-19	-17	-30	14
	all	0	8	-13	-23	-6	-12	-19	20
$C^{\text{tot}}$	WP	20	8	-92	15	8	2	3	22
	SP	31	-7	-57	-28	-16	-9	-9	-3
	all	26	0	-72	-10	-7	-4	-4	8
$P_{\text{Iasc}}$	WP	23	26	34	19	24	23	18	26
	SP	-1	-5	-14	5	3	-3	0	4
	all	8	6	4	10	11	6	6	12
$P_{\text{conv}}$	WP	—	100	—	—	—	—	—	—
	SP	30	6	-14	28	4	12	10	4
	all	30	8	-14	28	4	12	10	4
$P_{\text{snow}}$	WP	24	25	19	17	25	23	18	27
	SP	17	15	-59	3	17	13	15	18
	all	19	19	-22	9	20	17	16	22

4.1. Modified Adjustment Parameters of PS-Scheme

As introduced by Section 2.2 the PS-Scheme includes the two adjustment parameters  $\tilde{q}_0$  and  $K$ . The former was varied in the co-domain  $1 < \tilde{q}_0 \leq 20$ , following the restrictions  $\tilde{p} > 1$  and  $\tilde{q} > 1$  for the beta

distribution shape parameters to obtain only unimodal distributions. Also according to Tompkins [45], the conditions  $\tilde{q}_0 = \tilde{p}$  and  $\tilde{p} \leq \tilde{q}$  were retained to exclude distributions with negative skewness.

**Figure 5.** Difference plots (SENS minus CTRL) of simulated fractional cloud cover (*top*), cloud water content (*middle*), and cloud ice content (*bottom*) for one lower value of the PS-Scheme adjustment parameter  $\tilde{q}_0$  (*left column*) and one higher value of the tunable parameter  $CW_{\min}$  (*right column*), with  $\tilde{q}_0^{\text{def}} = 2$  and  $CW_{\min}^{\text{def}} = 0.1 \text{ mg kg}^{-1}$ . These sensitivity experiments were conducted at the NP-35 start position simulating from 1 August 2007 to 31 August 2008 by analogy to the reference run (Figure 3).



The third column of Tables 4 and 5 reveal that overall a lower (higher) value of  $\tilde{q}_0$  leads to a reduction of (rise in)  $C^{\text{tot}}$ . Indeed mid- and high-level clouds decrease significantly due to lower parameter values while low-level clouds tend to slightly increase (see Figure 5(a)). One possible reason for the increase at lower levels might be very low saturation water contents due to cold temperatures in the relatively wet boundary layer over the Arctic Ocean favoring cloud formation. Although lower values of  $\tilde{q}_0$  are able to reduce  $C^{\text{tot}}$  and rise IWP (overall increase in  $q_i$  suggested by Figure 5(c)) as well as  $P_{\text{snow}}$ , the overestimation of LWP is strengthened (overall increase in  $q_l$  suggested by Figure 5(e)). Both  $P_{\text{asc}}$  and  $P_{\text{conv}}$  rise amplifying the overestimation of  $P^{\text{tot}}$  as well.

The second adjustment parameter  $K$ , which relates the increase in the skewness parameter  $\tilde{q}$  to the detrainment of cloud condensate, was varied in the co-domain  $0 \leq K \leq 10,000$ . However, modifying this parameter only leads to temporary local changes of  $C$  (not shown), and overall  $C^{\text{tot}}$  remains almost unaffected. This can be attributed to the minor role of convection in cloud formation over the ice-covered Arctic Ocean, unless open water areas in terms of polynyas or leads coexist. Other cloud-related model variables either remain almost unchanged or increase in part significantly by changes in  $K$ . Both the overestimation of  $q_l$  (LWP) and  $P^{\text{tot}}$  is strengthened. Furthermore, only higher parameter values of  $K$  enable convective precipitation during wintertime (WP) explaining the increase of 100% in the fourth column of Table 5.

#### 4.2. Modified Tuning Parameters of Cloud Microphysics

The following discussions will basically concentrate on tuning parameters of the cloud microphysics, which can reduce  $C^{\text{tot}}$  based on Tables 4 and 5, and conclusions are summarized in Table 6.

**Table 6.** Overall effect on cloud-related model variables due to modification of a single model tuning parameter enabling the reduction of  $C^{\text{tot}}$  relative to the default parameter value (see Table 1 and Figure 4). Effects that potentially improve model results are marked by a ‘+’, negative influences are indicated by a ‘−’.

Parameter	Changes due to lower parameter value	Changes due to higher parameter value
$\tilde{q}_0$	1.5 + reduction of $C$ and $C^{\text{tot}}$ + rise in $q_i$ (IWP) − rise in $q_l$ (LWP) − rise in $P_{\text{asc}}$ and $P_{\text{conv}}$	20 + rise in $q_i$ (IWP) but reduction of $q_l$ (LWP); effect is small (large) for $q_l$ ( $q_i$ ) − rise in $C$ , $C^{\text{tot}}$ , $P_{\text{asc}}$ , and $P_{\text{conv}}$
$CW_{\text{min}}$	$7.5 \times 10^{-4} \text{ mg kg}^{-1}$ + rise in $q_i$ (IWP) but reduction of $q_l$ (LWP); effect is more pronounced than for higher $\tilde{q}_0$ and more significant for $q_i$ − rise in $C$ , $C^{\text{tot}}$ , $P_{\text{asc}}$ , and $P_{\text{conv}}$	$250 \text{ mg kg}^{-1}$ + significant reduction of $C$ , $C^{\text{tot}}$ + reduction of $P_{\text{conv}}$ − reduction of $q_i$ (IWP) but rise in $q_l$ (LWP) and $P_{\text{asc}}$
$\gamma_1$	5 + $q_i$ (IWP) rises but reduction of $P_{\text{conv}}$ − rise in all other regarded model variables	100 + rise in $q_i$ (IWP) but reduction of $q_l$ (LWP); effect is large (small) for $q_l$ ( $q_i$ ) + significant decrease in $C$ , $C^{\text{tot}}$ − rise in $P_{\text{asc}}$ and $P_{\text{conv}}$

Table 6. Cont.

Parameter	Changes due to lower parameter value	Changes due to higher parameter value
$\gamma_{\text{thr}}$	0.05 mg kg <sup>-1</sup> + rise in $q_i$ (IWP) but reduction of $q_l$ (LWP), where effect is significant for $q_l$ and $q_i$ + reduction of $C$ , $C^{\text{tot}}$ – increase in $P_{\text{lasc}}$ and $P_{\text{conv}}$	1 mg kg <sup>-1</sup> + $q_i$ (IWP) rises – rise in all remaining model variables

To assess the impact of modified  $CW_{\text{min}}$ , sensitivity experiments were conducted in the wide range between zero and 750 mg kg<sup>-1</sup>. Note that  $CW_{\text{min}}$  impacts model results by ensuring nonzero  $q_l$  and  $q_i$  regardless of the applied cloud scheme (see Table 1). As a working hypothesis, lower (higher)  $CW_{\text{min}}$  should result in rising (declining) cloud cover. This is generally confirmed by the fifth column of Tables 4 and 5. Higher  $CW_{\text{min}}$  lead to significant decrease in  $C^{\text{tot}}$ , and very high parameter values are even able to prevent the formation of clouds. While low- and high-level clouds tend to decline monotonically, mid-level clouds first seem to increase but finally decrease as well (suggested by Figure 5(b)). Despite the ability to reduce the overestimation of  $C^{\text{tot}}$ , higher  $CW_{\text{min}}$  amplify the over- and underestimation of LWP and IWP, respectively. During the entire simulation period  $q_l$  decreases below 900 h but significantly increases above 900 h, while  $q_i$  decreases monotonically (see Figure 5(d,f)). Furthermore, higher  $CW_{\text{min}}$  amplify the overestimation of  $P_{\text{lasc}}$  while  $P_{\text{conv}}$  and  $P_{\text{snow}}$  drop.

The autoconversion rate  $\gamma_1$ , which controls the conversion from (supercooled) cloud droplets to rain drops and thus the cloud lifetime effect, was found to be the next promising tuning parameter. This parameter was varied in the co-domain  $0 \leq \gamma_1 \leq 500$ . Figure 6(a) and the sixth column of Tables 4 and 5 confirm that only higher parameter values might be able to improve simulated cloudiness. Here, the increase in  $C^{\text{tot}}$  during wintertime (WP) is outweighed by the decrease during summertime (SP). Furthermore, higher  $\gamma_1$  are able to reduce the over- and underestimation of LWP and IWP, respectively. For  $q_l$  and  $q_i$  this effect is more difficult to identify from Figure 6(c,e) due to temporary local changes. As expected,  $P_{\text{lasc}}$  and  $P_{\text{conv}}$  rise in case of higher  $\gamma_1$  amplifying the overestimation of  $P^{\text{tot}}$ , while  $P_{\text{snow}}$  is more or less unaffected.

Finally, the cloud ice threshold  $\gamma_{\text{thr}}$  was identified as promising tuning parameter. This parameter controls the Bergeron–Findeisen process, which explains the growth of ice crystals at the expense of cloud droplets in mixed-phase clouds due to lower vapor pressures over ice than over water at subfreezing temperatures. Lohmann *et al.* [66] have pointed out that as soon as the threshold of cloud ice content is exceeded a supercooled water cloud will glaciate immediately in the model. In the standard ECHAM5 code the remaining cloud water is not evaporated to deposit onto existing ice crystals but remaining cloud droplets have to either freeze or grow to precipitable sizes in subsequent time steps. For the sake of completeness  $\gamma_{\text{thr}}$  was varied from zero to 5 mg kg<sup>-1</sup>. As shown by Figure 6(b) and the last column of Tables 4 and 5, lower  $\gamma_{\text{thr}}$  are also able to reduce the overestimation of simulated Arctic clouds. Furthermore, a lower parameter value is most suitable to improve the modeled ratio of  $q_l$  to  $q_i$  (overall reduction of  $q_l$  but rise in  $q_i$ , see Figure 6(d,f)), which can be associated with the most significant

reduction of LWP but rise in IWP. While  $C^{\text{tot}}$  decreases and  $P^{\text{tot}}$  remains almost unchanged,  $P_{\text{snow}}$  increases overall.

**Figure 6.** Difference plots (SENS minus CTRL) of simulated fractional cloud cover (*top*), cloud water content (*middle*), and cloud ice content (*bottom*) for one higher value of the tunable parameter  $\gamma_1$  (*left column*) and one lower value of the tunable parameter  $\gamma_{\text{thr}}$  (*right column*), with  $\gamma_1^{\text{def}} = 15$  and  $\gamma_{\text{thr}}^{\text{def}} = 0.5 \text{ mg kg}^{-1}$ . These sensitivity experiments were conducted at the NP-35 start position simulating from 1 August 2007 to 31 August 2008 by analogy to the reference run (Figure 3).

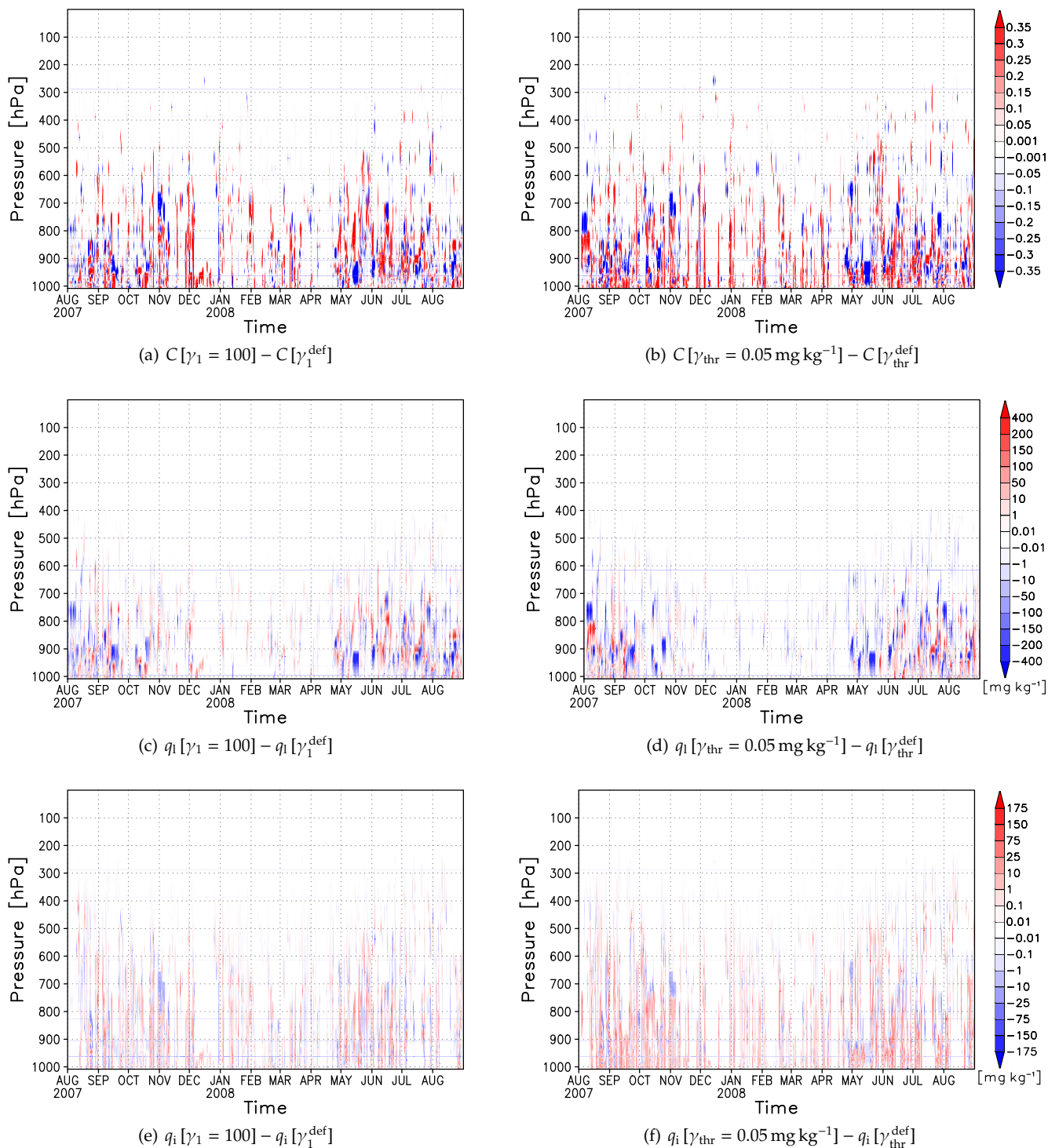


Figure 7 shows the comparison of monthly averaged  $C^{tot}$  by analogy to Section 3.2.2. Here, only the annual cycles of the best-fit parameters (*green curves*), based on the best combination of lowest 13-month-mean of  $C^{tot}$  and overall RMSE, are shown in addition to the annual cycle produced by MODIS (*black curve*) and using the default values (*blue curve*), respectively. Note that MODIS and the HIRHAM5-SCM reference run (using the PS-Scheme) produced averaged  $C^{tot}$  of 64.8% and 78.2%, respectively with an overall RMSE of 18.4% (see Table 3). Thus, Figure 7 confirms that higher  $CW_{min}$  (averaged  $C^{tot}$  of 77.3% and overall RMSE of 17.2% for  $CW_{min} = 1 \text{ mg kg}^{-1}$ ) and  $\gamma_1$  (averaged  $C^{tot}$  of 77.8% and overall RMSE of 17.3% for  $\gamma_1 = 100$ ) as well as lower  $\tilde{q}_0$  (averaged  $C^{tot}$  of 76.5% and overall RMSE of 17.9% for  $\tilde{q}_0 = 1.5$ ) and  $\gamma_{thr}$  (averaged  $C^{tot}$  of 74.9% and overall RMSE of 14.1% for  $\gamma_{thr} = 0.05 \text{ mg kg}^{-1}$ ) reduce simulated Arctic cloud cover, where the latter might be the most promising tuning parameter to improve cloud-related variables in the model.

**Figure 7.** Monthly means of  $C^{tot}$  (in %) from August 2007 to August 2008 referring to the NP-35 start position. The results originate from MODIS (*black line*) satellite observations, and HIRHAM5-SCM simulations using either the PS-Scheme and default model parameters (*blue line*) or the PS-Scheme with a single modified tuning parameter (*green lines*).

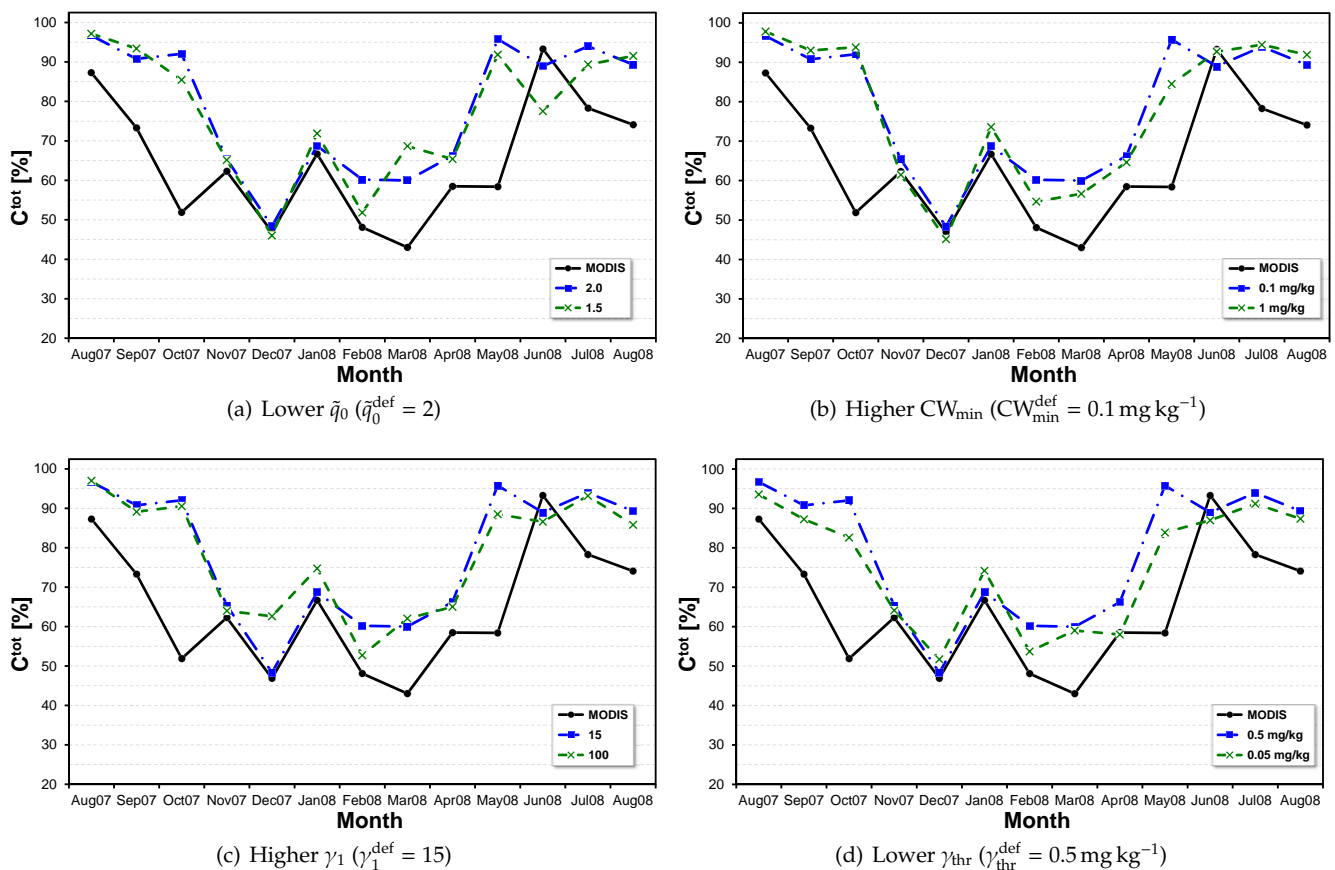


Figure 7 also reveals that all four tuning parameters are able to reduce  $C^{tot}$  during May 2008 while only modified  $\tilde{q}_0$  and  $\gamma_{thr}$  improve the simulation of Arctic clouds during October 2007. In the former case, the enhanced cloud formation due to unrealistic turbulent moisture fluxes could be either partially compensated due to more efficient precipitation processes (for  $\gamma_1$  and  $\gamma_{thr}$ ) or through the partial suppression of cloud formation (for  $\tilde{q}_0$  and  $CW_{min}$ ). In the latter case, both the more

deficient simulation of the ABL structure and the overestimated cloud top radiative cooling could not be significantly improved by changing tuning parameters of the cloud microphysics, except for  $\gamma_{\text{thr}}$ . The most significant impact through reduced  $\gamma_{\text{thr}}$  in both cases can be explained with the more efficient Bergeron–Findeisen process which results in faster growing cloud ice particles and finally enhanced snow fall.

## 5. Conclusions

A SCM version of the atmospheric RCM HIRHAM5 was developed to analyze the representation of Arctic clouds. HIRHAM5-SCM was exploited as test bed for evaluating the cloud cover schemes of the ECHAM5 parameterization package, the RH-Scheme by Sundquist *et al.* [52] and the more sophisticated PS-Scheme by Tompkins [45].

Observations from the 35th Russian North Pole drifting station (NP-35) were used to validate the model. Above the Arctic boundary layer (ABL), simulated and observed temperature profiles agree fairly well. In contrast, the more pronounced vertical variability of relative humidity is inadequately reproduced. Primarily the RH-Scheme produces clouds at incorrect altitudes. The PS-Scheme enables to better simulate the observed correlation between the occurrence of boundary layer clouds (BLCs) and capping strong temperature inversion as well as rapid moisture decrease. Further, the PS-Scheme results in higher correlations between the simulated and the measured temperature and humidity profiles. Nevertheless, the model has difficulties in simulating the ABL, most likely due to unrealistic turbulent exchange under extremely stable conditions.

The evaluation of relative frequencies of simulated clear-sky, partially cloudy, and (totally) overcast cases revealed underestimation of clear-sky and overestimation of overcast conditions as compared to ground-based observations at NP-35. Both biases are significantly larger when using the RH-Scheme, even though the frequency of partially cloudy conditions agrees well. Overall, the overestimation of cloudy cases (sum of partially cloudy and overcast cases) is reduced by the PS-Scheme.

Independent from the used cloud scheme, the higher frequency of occurrence of modeled low-level clouds during summer (JJA) and autumn (SON) is in accordance with the frequently observed presence of summertime BLCs [13,14]. However, the PS-Scheme simulates cloud formation and dissipation more realistically, since the cloud cover is directly linked to sources and sinks (like turbulence, convection, and microphysics), enabling the simulation of frequently observed abrupt changes between overcast and clear-sky conditions.

The validation of the simulated annual cycle of total cloud cover against ISCCP-D2 and MODIS satellite observations showed qualitative agreement with MODIS in terms of higher cloud cover in summer and lower cloud cover in winter. The annual cycle of ISCCP-D2 is reversed and might be unrealistic as has already been pointed out by Schweiger *et al.* [71] and as is suggested by comparison with the ground-based observations at NP-35.

The qualitative agreement with MODIS is independent from the cloud cover scheme, but the RH-Scheme systematically overestimates the cloud cover, while the PS-Scheme shows reduced biases and pretty good agreement from November to January. However, the transition from high cloud cover

in summer to lower cloud cover in winter and *vice versa* is shifted to the cold season in either case, accompanied by large biases in October and May.

All in all, the PS-Scheme enables an improved simulation of Arctic clouds as compared to the RH-Scheme, but it still shows a systematic overestimation of Arctic cloud cover. Several tunable parameters were analyzed by means of sensitivity studies to identify parameters which potentially enable the adaptation of the cloud parameterization to Arctic climate conditions. The resulting recommendations are summarized below:

- Lower values of  $\tilde{q}_0$ , the parameter that determines the shape of the symmetric beta distribution in the PS-Scheme, result in a reduction of total cloud cover ( $\tilde{q}_0 = 1.5$  best fit to MODIS), decreased underestimation of cloud ice, but increased overestimation of cloud water and precipitation.
- Higher values of the minimum cloud water content  $CW_{\min}$  result in a reduction of clouds (even up to their total disappearance) and consequently decreased overestimation of total cloud cover ( $CW_{\min} = 1 \text{ mg kg}^{-1}$  best fit to MODIS), but also in increased overestimation/underestimation of cloud water/cloud ice and increased overestimation of precipitation. Instead of applying the same value of  $CW_{\min}$  to cloud water and cloud ice, it is suggested using different thresholds, since cloud water contents are typically about one magnitude higher than cloud ice contents in Arctic clouds (e. g., [28,47]).
- Higher values of the autoconversion rate  $\gamma_1$ , which controls the local rain production and thus the cloud lifetime, result in decreased overestimation of total cloud cover ( $\gamma_1 = 100$  best fit to MODIS), decreased overestimation/underestimation of cloud water/cloud ice, but increased overestimation of precipitation as was expected.
- Lower values of the cloud ice threshold  $\gamma_{\text{thr}}$ , which controls the efficiency of the Bergeron–Findeisen process, turned out to be most suitable for reducing the overestimation of total cloud cover ( $\gamma_{\text{thr}} = 0.05 \text{ mg kg}^{-1}$  best fit to MODIS) and result additionally in decreased overestimation/underestimation of cloud water/cloud ice, but also increased overestimation of precipitation.

The best-fit parameters suggested by this study need to be examined for their performance in the three-dimensional model version HIRHAM5. Liu *et al.* [77] have identified the possible underestimation of MODIS relative to CloudSat-CALIPSO cloud amount especially over the ice-covered Arctic ocean. It is therefore planned to validate cloud-related variables simulated by HIRHAM5 against observations from the Multiangle Imaging SpectroRadiometer (MISR) and Cloud Aerosol Lidar with Orthogonal Polarization (CALIOP). Since changes in modeled cloud fraction and total precipitation are anti-correlated, extensive validation against precipitation observations is required. This is currently ongoing work.

## Acknowledgments

Financial support was provided by the Helmholtz Climate Initiative REKLIM. The authors thank the ECMWF for providing the ERA-Interim data set and Ines Hebestadt for technical support. We are deeply

grateful to the ISCCP for providing ISCCP-D2 and to the NSIDC for providing MODIS satellite cloud data. Special thanks go to the Arctic and Antarctic Research Institute (AARI) St. Petersburg, Russia, and Jürgen Gräser for the measurements on NP-35.

## References

1. Schneider, S.H. Cloudiness as a global climate feedback mechanism: The effects on the radiation balance and surface temperature of variations in cloudiness. *J. Atmos. Sci.* **1972**, *29*, 1413–1422.
2. Minnett, P.J. The influence of solar zenith angle and cloud type on cloud radiative forcing at the surface in the Arctic. *J. Clim.* **1999**, *12*, 147–158.
3. Shupe, M.D.; Intrieri, J.M. Cloud radiative forcing of the Arctic surface: The influence of cloud properties, surface albedo, and solar zenith angle. *J. Clim.* **2004**, *17*, 616–628.
4. Hu, R.M.; Blanchet, J.P.; Girard, E. The effect of aerosol on surface cloud radiative forcing in the Arctic. *Atmos. Chem. Phys. Discuss.* **2005**, *5*, doi:10.5194/acpd-5-9039-2005.
5. Gorodetskaya, I.V.; Tremblay, L.B.; Liepert, B.; Cane, M.A.; Cullather, R.I. The influence of cloud and surface properties on the Arctic ocean shortwave radiation budget in coupled models. *J. Clim.* **2008**, *21*, doi:10.1175/2007JCLI1614.1.
6. Lee, S.S.; Donner, L.J.; Phillips, V.T.J. Sensitivity of aerosol and cloud effects on radiation to cloud types: Comparison between deep convective clouds and warm stratiform clouds over one-day period. *Atmos. Chem. Phys.* **2009**, *9*, doi:10.5194/acp-9-2555-2009.
7. Ramanathan, V.; Cess, R.D.; Harrison, E.F.; Minnis, P.; Barkstrom, B.R.; Ahmad, E.; Hartmann, D. Cloud-radiative forcing and climate: Results from the earth radiation budget experiment. *Science* **1989**, *243*, 57–63.
8. Walsh, J.E.; Chapman, W.L. Arctic cloud-radiation-temperature associations in observational data and atmospheric reanalyses. *J. Clim.* **1998**, *11*, 3030–3045.
9. Intrieri, J.M.; Fairall, C.W.; Shupe, M.D.; Persson, P.O.G.; Andreas, E.L.; Guest, P.S.; Moritz, R.E. An annual cycle of Arctic surface cloud forcing at SHEBA. *J. Geophys. Res.* **2002**, *107*, doi:10.1029/2000JC000439.
10. Kahl, J.D.; Martinez, D.A.; Zaitseva, N.A. Long-term variability in the low-level inversion layer over the Arctic ocean. *Int. J. Climatol.* **1996**, *16*, 1297–1313.
11. Zhang, Y.; Seidel, D.J.; Golaz, J.C.; Deser, C.; Tomas, R.A. Climatological characteristics of Arctic and Antarctic surface-based inversions. *J. Clim.* **2011**, *24*, doi:10.1175/2011JCLI4004.1.
12. Mauritsen, T.; Sedlar, J.; Tjernström, M.; Leck, C.; Martin, M.; Shupe, M.; Sjogren, S.; Sierau, B.; Persson, P.O.G.; Brooks, I.M.; *et al.* An Arctic CCN-limited cloud-aerosol regime. *Atmos. Chem. Phys.* **2011**, *11*, doi:10.5194/acp-11-165-2011.
13. Herman, G.; Goody, R. Formation and persistence of summertime Arctic stratus clouds. *J. Atmos. Sci.* **1976**, *33*, 1537–1553.
14. Curry, J.A.; Rossow, W.B.; Randall, D.; Schramm, J.L. Overview of Arctic cloud and radiative characteristics. *J. Clim.* **1996**, *9*, 1731–1764.
15. Intrieri, J.M.; Shupe, M.D.; Uttal, T.; McCarty, B.J. An annual cycle of Arctic cloud characteristics observed by radar and lidar at SHEBA. *J. Geophys. Res.* **2002**, *107*, doi:10.1029/2000JC000423.

16. Kay, J.E.; Gettelman, A. Cloud influence on and response to seasonal Arctic sea ice loss. *J. Geophys. Res.* **2009**, *114*, doi:10.1029/2009JD011773.
17. Eastman, R.; Warren, S.G. Interannual variations of Arctic cloud types in relation to sea ice. *J. Clim.* **2010**, *23*, doi:10.1175/2010JCLI3492.1.
18. Eastman, R.; Warren, S.G. Arctic cloud changes from surface and satellite observations. *J. Clim.* **2010**, *23*, doi:10.1175/2010JCLI3544.1.
19. Walsh, J.E.; Kattsov, V.M.; Chapman, W.L.; Govorkova, V.; Pavlova, T. Comparison of Arctic climate simulations by uncoupled and coupled global models. *J. Clim.* **2002**, *15*, 1429–1446.
20. Inoue, J.; Liu, J.; Pinto, J.O.; Curry, J.A. Intercomparison of Arctic regional models: Modeling clouds and radiation for SHEBA in May 1998. *J. Clim.* **2006**, *19*, doi:10.1175/JCLI3854.1.
21. Tjernström, M.; Sedlar, J.; Shupe, M.D. How well do regional climate models reproduce radiation and clouds in the Arctic? An evaluation of ARCMIP simulations. *J. Appl. Meteorol. Climatol.* **2008**, *47*, doi:10.1175/2008JAMC1845.1.
22. Birch, C.E.; Brooks, I.M.; Tjernström, M.; Milton, S.F.; Earnshaw, P.; Soderberg, S.; Persson, P.O.G. The performance of a global and mesoscale model over the central Arctic ocean during late summer. *J. Geophys. Res.* **2009**, *114*, doi:10.1029/2008JD010790.
23. Arking, A. The radiative effects of clouds and their impact on climate. *Bull. Am. Meteorol. Soc.* **1991**, *71*, 795–813.
24. Cess, R.D.; Zhang, M.H.; Ingram, W.J.; Potter, G.L.; Alekseev, V.; Barker, H.W.; Cohen-Solal, E.; Colman, R.A.; Dazlich, D.A.; Del Genio, A.D.; *et al.* Cloud feedback in atmospheric general circulation models: An update. *J. Geophys. Res.* **1996**, *101*, doi:10.1029/96JD00822.
25. Solomon, S.; Qin, D.; Manning, M.; Chen, Z.; Marquis, M.; Averyt, K.B.; Tignor, M.; Miller, H.L. *Climate Change 2007: The Physical Science Basis: Contribution of Working Group I to the Fourth Assessment Report of the Intergovernmental Panel on Climate Change*; Cambridge University Press: Cambridge, UK, 2007; pp. 629–640.
26. Curry, J.A.; Pinto, J.O.; McInnes, K.L. Modeling the Summertime Arctic Cloudy Boundary Layer. In *Proceedings of the Fifth Atmospheric Radiation Measurement (ARM) Science Team Meeting; Department of Energy/Atmospheric Radiation Measurement (DOE/ARM)*, San Diego, CA, USA, 19–23 March 1995; pp. 63–67.
27. Morrison, H.; Pinto, J.O. Intercomparison of bulk cloud microphysics schemes in mesoscale simulations of springtime Arctic mixed-phase stratiform clouds. *Mon. Weather Rev.* **2006**, *134*, 1880–1900.
28. Sednev, I.; Menon, S.; McFarquhar, G. Simulating mixed-phase Arctic stratus clouds: Sensitivity to ice initiation mechanisms. *Atmos. Chem. Phys.* **2009**, *9*, doi:10.5194/acp-9-4747-2009.
29. Inoue, J.; Kosovic, B.; Curry, J.A. Evolution of a storm-driven cloudy boundary layer in the Arctic. *Bound. Layer Meteorol.* **2005**, *117*, doi:10.1007/s10546-004-6003-2.
30. Wyser, K.; Jones, C.G.; Du, P.; Girard, E.; Willén, U.; Cassano, J.; Christensen, J.H.; Curry, J.A.; Dethloff, K.; Haugen, J.E.; *et al.* An evaluation of Arctic cloud and radiation processes during the SHEBA year: Simulation results from eight Arctic regional climate models. *Clim. Dyn.* **2008**, *30*, doi:10.1007/s00382-007-0286-1.

31. Luo, Y.; Xu, K.M.; Morrison, H.; McFarquhar, G. Arctic mixed-phase clouds simulated by a cloud-resolving model: Comparison with ARM observations and sensitivity to microphysics parameterizations. *J. Atmos. Sci.* **2008**, *65*, doi:10.1175/2007JAS2467.1.
32. Klein, S.A.; McCoy, R.B.; Morrison, H.; Ackerman, A.S.; Avramov, A.; de Boer, G.; Chen, M.; Cole, J.N.S.; Del Genio, A.D.; Falk, M.; *et al.* Intercomparison of model simulations of mixed-phase clouds observed during the ARM mixed-phase Arctic cloud experiment. I: Single-layer cloud. *Q. J. R. Meteorol. Soc.* **2009**, *135*, doi:10.1002/qj.416.
33. Lubin, D.; Vogelmann, A.M. A climatologically significant aerosol longwave indirect effect in the Arctic. *Nature* **2006**, *439*, 453–456.
34. Garrett, T.J.; Zhao, C. Increased Arctic cloud longwave emissivity associated with pollution from mid-latitudes. *Nature* **2006**, *440*, 787–789.
35. Morrison, H.; Pinto, J.O.; Curry, J.A.; McFarquhar, G.M. Sensitivity of modeled Arctic mixed-phase stratocumulus to cloud condensation and ice nuclei over regionally varying surface conditions. *J. Geophys. Res.* **2008**, *113*, doi:10.1029/2007JD008729.
36. Morrison, H.; McCoy, R.B.; Klein, S.A.; Xie, S.; Luo, Y.; Avramov, A.; Chen, M.; Cole, J.N.S.; Falk, M.; Foster, M.J.; *et al.* Intercomparison of model simulations of mixed-phase clouds observed during the ARM mixed-phase Arctic cloud experiment. II: Multilayer cloud. *Q. J. R. Meteorol. Soc.* **2009**, *135*, doi:10.1002/qj.415.
37. Hannay, C.; Bhatt, U.S.; Harrington, J.Y. Single-Column Model Simulations of Arctic Cloudiness and Surface Radiative Fluxes during the Surface Heat Budget of the Arctic (SHEBA) Experiment. In *Proceedings of the 6th Conference on Polar Meteorology and Oceanography; American Meteorological Society (AMS)*, San Diego, CA, USA, 14–18 May 2001.
38. Kay, J.E.; Raeder, K.; Gettelman, A.; Anderson, J. The boundary layer response to recent Arctic sea ice loss and implications for high-latitude climate feedbacks. *J. Clim.* **2011**, *24*, doi:10.1175/2010JCLI3651.1.
39. Pinto, J.O.; Curry, J.A. Atmospheric convective plumes emanating from leads 2. Microphysical and radiative processes. *J. Geophys. Res.* **1995**, *100*, 4633–4642.
40. Curry, J.A.; Hobbs, P.V.; King, M.D.; Randall, D.A.; Minnis, P.; Isaac, G.A.; Pinto, J.O.; Uttal, T.; Bucholtz, A.; Cripe, D.G.; *et al.* FIRE Arctic clouds experiment. *Bull. Am. Meteorol. Soc.* **2000**, *81*, 5–29.
41. Rozwadowska, A.; Cahalan, R.F. Plane-parallel biases computed from inhomogeneous Arctic clouds and sea ice. *J. Geophys. Res.* **2002**, *107*, doi:10.1029/2002JD002092.
42. Sato, K.; Inoue, J.; Kodama, Y.M.; Overland, J.E. Impact of Arctic sea-ice retreat on the recent change in cloud-base height during autumn. *Geophys. Res. Lett.* **2012**, *39*, doi:10.1029/2012GL051850.
43. Lohmann, U.; Roeckner, E. Design and performance of a new cloud microphysics parametrization developed for the ECHAM general circulation model. *Clim. Dyn.* **1996**, *12*, 557–572.
44. Salzmann, M.; Ming, Y.; Golaz, J.C.; Ginoux, P.A.; Morrison, H.; Gettelman, A.; Krämer, M.; Donner, L.J. Two-moment bulk stratiform cloud microphysics in the GFDL AM3 GCM: Description, evaluation, and sensitivity tests. *Atmos. Chem. Phys.* **2010**, *10*, doi:10.5194/acp-10-8037-2010.

45. Tompkins, A.M. A prognostic parameterization for the subgrid-scale variability of water vapor and clouds in large-scale models and its use to diagnose cloud cover. *J. Atmos. Sci.* **2002**, *59*, 1917–1942.
46. Zhu, P.; Zuidema, P. On the use of PDF schemes to parameterize sub-grid clouds. *Geophys. Res. Lett.* **2009**, *36*, doi:10.1029/2008GL036817.
47. Pinto, J.O.; Curry, J.A.; Lynch, A.H.; Persson, P.O.G. Modeling clouds and radiation for the November 1997 period of SHEBA using a column climate model. *J. Geophys. Res.* **1999**, *104*, doi:10.1029/98JD02517.
48. Dethloff, K.; Abegg, C.; Rinke, A.; Hebestadt, I.; Romanov, V.F. Sensitivity of Arctic climate simulations to different boundary layer parameterizations in a regional climate model. *Tellus A* **2001**, *53*, 1–26.
49. Zhang, J.; Lohmann, U. Sensitivity of single column model simulations of Arctic springtime clouds to different cloud cover and mixed phase cloud parameterizations. *J. Geophys. Res.* **2003**, *108*, doi:10.1029/2002JD003136.
50. Morrison, H.; Curry, J.A.; Shupe, M.D.; Zuidema, P. A new double-moment microphysics parameterization for application in cloud and climate models. part II: Single-column modeling of Arctic clouds. *J. Atmos. Sci.* **2005**, *62*, doi:10.1175/JAS3447.1.
51. *The HIRHAM Regional Climate Model Version 5( $\beta$ )*; Technical Report 06-17; Danish Meteorological Institute (DMI): Copenhagen, Denmark, 2007.
52. Sundquist, H.; Berge, E.; Kristjánsson, J.E. Condensation and cloud parameterization studies with a mesoscale numerical weather prediction model. *Mon. Weather Rev.* **1989**, *117*, 1641–1657.
53. Undén, P.; Rontu, L.; Järvinen, H.; Lynch, P.; Calvo, J.; Cats, G.; Cuxart, J.; Eerola, K.; Fortelius, C.; Garcia-Moya, J.A.; *et al.* HIRLAM-5 Scientific Documentation. In *HIRLAM-5 Project*; Swedish Meteorological and Hydrological Institute (SMHI): Norrköping, Sweden, 2002.
54. *The Atmospheric General Circulation Model ECHAM5–Part I: Model Description*; Technical Report 349; Max Planck Institute (MPI) for Meteorology: Hamburg, Germany, 2003.
55. *The ERA–Interim Archive*; ERA report series; European Center for Medium-Range Weather Forecasts (ECMWF): Reading, UK, 2009.
56. Bergman, J.W.; Sardeshmukh, P.D. Dynamic stabilization of atmospheric single column models. *J. Clim.* **2004**, *17*, 1004–1021.
57. Dee, D.P.; Uppala, S.M.; Simmons, A.J.; Berrisford, P.; Poli, P.; Kobayashi, S.; Andrae, U.; Balmaseda, M.A.; Balsamo, G.; Bauer, P.; *et al.* The ERA-Interim reanalysis: Configuration and performance of the data assimilation system. *Q. J. R. Meteorol. Soc.* **2011**, *137*, 553–597.
58. Randall, D.A.; Cripe, D.G. Alternative methods for specification of observed forcing in single-column models and cloud system models. *J. Geophys. Res.* **1999**, *104*, doi:10.1029/1999JD900765.
59. Lohmann, U.; McFarlane, N.; Levkov, L.; Abdella, K.; Albers, F. Comparing different cloud schemes of a single column model by using mesoscale forcing and nudging technique. *J. Clim.* **1999**, *12*, 438–461.

60. Atmospheric Investigations on the Russian North Pole Drifting Ice Station NP-35. Available online: [http://www.awi.de/en/research/research\\_divisions/climate\\_science/atmospheric\\_circulations/expeditions\\_campaigns/np\\_35/](http://www.awi.de/en/research/research_divisions/climate_science/atmospheric_circulations/expeditions_campaigns/np_35/) (accessed on 9 August 2012).
61. *The Atmospheric General Circulation Model ECHAM4: Model Description and Simulation of Present-Day Climate*; Technical Report 218; Max Planck Institute (MPI) for Meteorology: Hamburg, Germany, 1996.
62. Wild, M.; Roeckner, E. Radiative fluxes in the ECHAM5 general circulation model. *J. Clim.* **2006**, *19*, doi:10.1175/JCLI3823.1.
63. Tiedtke, M. A comprehensive mass flux scheme for cumulus parameterization in large-scale models. *Mon. Weather Rev.* **1989**, *117*, 1179–1800.
64. Nordeng, T.E. Extended Versions of the Convective Parametrization Scheme at ECMWF and Their Impact on the Mean and Transient Activity of the Model in the Tropics. In *Technical Memorandum*; European Center for Medium-Range Weather Forecasts (ECMWF): Reading, UK, 1994.
65. Wang, S.; Wang, Q.; Jordan, R.E.; Persson, P.O.G. Interactions among longwave radiation of clouds, turbulence, and snow surface temperature in the Arctic: A model sensitivity study. *J. Geophys. Res.* **2001**, *106*, doi:10.1029/2000JD900358.
66. Lohmann, U.; Stier, P.; Hoose, C.; Ferrachat, S.; Kloster, S.; Roeckner, E.; Zhang, J. Cloud microphysics and aerosol indirect effects in the global climate model ECHAM5-HAM. *Atmos. Chem. Phys.* **2007**, *7*, 3425–3446.
67. Rossow, W.B.; Schiffer, R.A. Advances in understanding clouds from ISCCP. *Bull. Am. Meteorol. Soc.* **1999**, *80*, 2261–2287.
68. International Satellite Cloud Climatology Project (ISCCP) by NASA Goddard Institute for Space Studies (GISS). Available online: <ftp://isccp.giss.nasa.gov/pub/data/D2Tars/> (accessed on 25 August 2011).
69. MODIS Atmosphere L3 Gridded Product Algorithm Theoretical Basis Document. Available online: [http://modis-atmos.gsfc.nasa.gov/\\_docs/MOD08MYD08%20ATBD%20C005.pdf](http://modis-atmos.gsfc.nasa.gov/_docs/MOD08MYD08%20ATBD%20C005.pdf) (accessed on 9 August 2012).
70. Moderate Resolution Imaging Spectroradiometer (MODIS) by National Aeronautics and Space Administration (NASA). Available online: [ftp://ladsweb.nascom.nasa.gov/allData/5/MOD08\\_M3/](ftp://ladsweb.nascom.nasa.gov/allData/5/MOD08_M3/) (accessed on 14 October 2011).
71. Schweiger, A.J.; Lindsay, R.W.; Key, J.R.; Francis, J.A. Arctic clouds in multilayer satellite data sets. *Geophys. Res. Lett.* **1999**, *26*, 1845–1848.
72. Hahn, C.J.; Warren, S.G.; London, J. The effect of moonlight on observations of cloud cover at night, and application to cloud climatology. *J. Clim.* **1995**, *8*, 1429–1466.
73. Wielicki, B.A.; Parker, L. On the determination of cloud cover from satellite sensors: The effect of sensor spatial resolution. *J. Geophys. Res.* **1992**, *97*, doi:10.1029/92JD01061.
74. Zhao, M.; Wang, Z. Comparison of Arctic clouds between European Center for Medium-Range Weather Forecasts simulations and Atmospheric Radiation Measurement Climate Research Facility long-term observations at the North Slope of Alaska Barrow Site. *J. Geophys. Res.* **2010**, *115*, doi:10.1029/2010JD014285.

75. Axelsson, P.; Tjernström, M.; Söderberg, S.; Svensson, G. An ensemble of Arctic simulations of the AOE-2001 field experiment. *Atmosphere* **2011**, *2*, doi:10.3390/atmos2020146.
76. Weber, T.; Quaas, J.; Räisänen, P. Evaluation of the statistical cloud scheme in the ECHAM5 model using satellite data. *Q. J. R. Meteorol. Soc.* **2011**, *137*, doi:10.1002/qj.887.
77. Liu, Y.; Ackerman, S.A.; Maddux, B.C.; Key, J.R.; Frey, R.A. Errors in cloud detection over the Arctic using a satellite imager and implications for observing feedback mechanisms. *J. Clim.* **2010**, *23*, doi:10.1175/2009JCLI3386.1.

© 2012 by the authors; licensee MDPI, Basel, Switzerland. This article is an open access article distributed under the terms and conditions of the Creative Commons Attribution license (<http://creativecommons.org/licenses/by/3.0/>).